Organizational Modes of Midlatitude Mesoscale Convective Systems

Matthew D. Parker and Richard H. Johnson

Department of Atmospheric Science, Colorado State University, Fort Collins, Colorado

ABSTRACT

This paper discusses common modes of mesoscale convective organization. Using 2-km national composite reflectivity data, the authors investigated linear mesoscale convective systems (MCSs) that occurred in the central United States during May 1996 and May 1997. Based upon the radar-observed characteristics of 88 linear MCSs, the authors propose a new taxonomy comprising convective lines with trailing (TS), leading (LS), and parallel (PS) stratiform precipitation. While the TS archetype was found to be the dominant mode of linear MCS organization, the LS and PS archetypes composed nearly 40% of the studied population. In this paper, the authors document the characteristics of each linear MCS class and use operational surface and upper air data to describe their different environments. In particular, wind profiler data reveal that the stratiform precipitation arrangement associated with each class was roughly consistent with the advection of hydrometeors implied by the mean middle- and upper-tropospheric storm-relative winds, which were significantly different among the three MCS modes. Case study examples are presented for both the LS and PS classes, which have received relatively little attention to this point. As well, the authors give a general overview of the synoptic-scale meteorology accompanying linear MCSs in this study, which was generally similar to that observed by previous investigators.

1. Introduction

Convective storms circulate mass and redistribute momentum and entropy in the troposphere. Conglomerates of convective storms are often organized on the mesoscale, behaving as long-lived ($\geq$3 h) discrete entities called mesoscale convective systems (MCSs). Given their ubiquity, the manner in which midlatitude MCSs respond to and force the large-scale environment is of particular interest. Nicholls et al. (1991) pointed out that the latent heating profiles of stratiform and convective precipitation regions each produce unique effects upon the circulation in the surrounding atmosphere. As well, LeMone and Moncrieff (1994) noted that to properly represent the effects of MCSs in large-scale models, the sensitivity of momentum fluxes to the ''structure of the mesoscale convective system and its environment'' must be known. The organization of MCSs is also important for hazardous weather forecasting and warning. Doswell et al. (1996) showed the relevance of precipitation arrangement to flash flooding associated with MCSs, for example. In this paper, we develop a classification of linear MCSs based upon their

distribution of stratiform[1] precipitation and discuss environmental thermodynamic and flow features associated with three common archetypes. If the conditions associated with various recurrent precipitation patterns are more clearly understood, both convective parameterizations and operational forecasting of MCSs can be improved.

a. Background

The relationship of organized convection to the surrounding environment has long been studied. Previous authors have analyzed MCS populations observed during field experiments [e.g., Barnes and Sieckman (1984) for the GARP Atlantic Tropical Experiment, Alexander and Young (1992) for the Equatorial Mesoscale Experiment, and LeMone et al. (1998) for the Tropical Ocean Global Atmosphere Coupled Ocean–Atmosphere Response Experiment (TOGA COARE)]. As well, a specific subset of MCSs known as mesoscale convective complexes (MCCs, as defined by Maddox 1980) has received a great deal of attention (e.g., Maddox 1983; Rodgers et al. 1983; McAnelly and Cotton 1986) due

---

Corresponding author address: Matthew Parker, Department of Atmospheric Science, Colorado State University, Fort Collins, CO 80523-1371.
E-mail: parker@squall.atmos.colostate.edu

[1] Although some authors (e.g., Doswell et al. 1996) have pointed out that secondary ''stratiform'' precipitation in MCSs may not always be truly stratiform in nature, we have retained the term due to its widespread usage in the published literature.
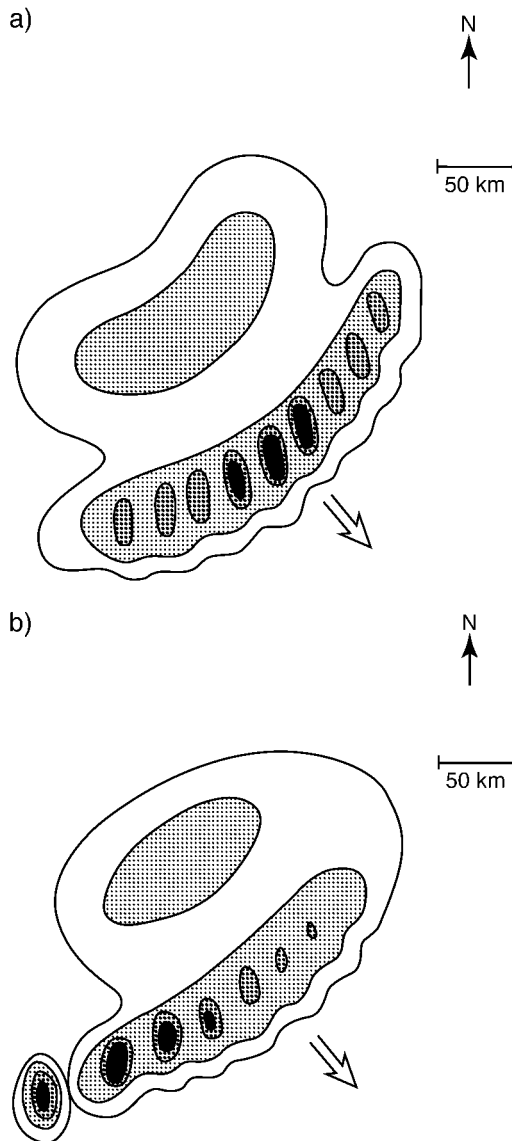
a)

N

50 km

b)

N

50 km

FIG. 1. Schematic reflectivity drawings of leading-line trailing-stratiform mesoscale precipitation systems, redrafted from Houze et al. (1990): (a) symmetric, and (b) asymmetric archetypes.

to its ease of identification from infrared satellite imagery. In addition, operational radar data have been investigated for recurrent mesoscale convective patterns. Bluestein and Jain (1985) and Bluestein et al. (1987) presented a taxonomy based upon squall lines' modes of development. They found that squall lines commonly formed via *broken line, backbuilding, broken areal,* and *embedded areal* pathways. Houze et al. (1990, hereafter HSD90) considered 63 *mesoscale precipitation systems* (whose characteristics were quite similar to those of MCSs in our study) that traversed the Norman, Oklahoma, Weather Surveillance Radar-57 range during the spring (April, May, and June) months of six successive years. HSD90 evaluated the degree to which

Occurrence of a large stratiform area at mature stage of MCS (25 - 40 dBZ widespread)

trailing   ahead   none

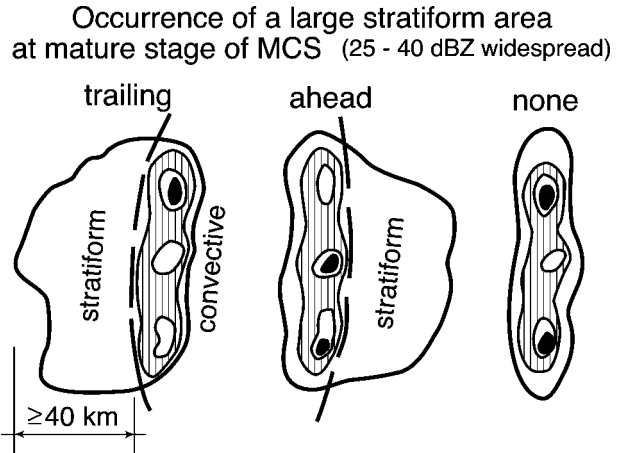stratiform   convective   stratiform

≥40 km

FIG. 2. Schematic reflectivity drawings of organizational archetypes for Swiss mesoscale convective systems, redrafted from Schiesser et al. (1995).

observed precipitation systems conformed to a *leading-line trailing-stratiform* (this mode is hereafter called TS) structural archetype as well as the degree to which MCSs were *symmetric* or *asymmetric* (Fig. 1). In a related effort, Schiesser et al. (1995, hereafter SHH95) documented the mesoscale structure of *severe precipitation systems* in Switzerland. In addition to the TS archetype, SHH95 noted the existence of precipitation systems with leading stratiform rain (this mode is hereafter called LS) as well as those with very little leading or trailing stratiform rain (Fig. 2). The above studies served as blueprints for the present work, and provided the foundation from which we proceeded.

b. Motivation

Moncrieff (1992) showed with an idealized analytical model that mature thunderstorm lines should exhibit both an ascending front-to-rear flow (called the *jump updraft*) and an *overturning updraft* directly above the leading edge of the surface outflow (Fig. 3). Fankhauser et al. (1992) correctly noted that while early work on convective lines frequently focused on systems with a significant overturning updraft and leading anvil cloudiness (e.g., Newton and Newton 1959; Newton and Fankhauser 1964; Newton 1966), the advent of MCS studies began increased attention to the front-to-rear

H

h

Jump

Ⓒ Overturning Updraught

h_o

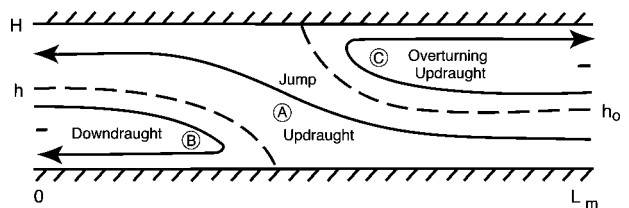Downdraught   Ⓑ   Ⓐ   Updraught

0   L_m

FIG. 3. Theoretical two-dimensional model of a convective line depicting both jump and overturning updrafts, redrafted from Moncrieff (1992).

movement of hydrometeors. Fovell and Dailey (1995) found that various modes of modeled multicell thunderstorms, regardless of regeneration periodicity, exhibited new convection near the leading edge of storm outflow, with subsequent upward and rearward motion within a canted updraft flow (first described by Ludlam 1963). This process results in the deposition of hydrometeors aft of the convective line (i.e., a TS structure). Indeed, many recent papers have addressed TS MCSs (e.g., Belair et al. 1995; Caniaux et al. 1995; Gallus and Johnson 1995a,b; Hane and Jorgensen 1995; Loehrer and Johnson 1995; Yang and Houze 1995, 1996; Braun and Houze 1995, 1997; Hilgendorf and Johnson 1998; Knupp et al. 1998a,b). As well, HSD90 found that a majority of the mesoscale precipitation systems in Oklahoma during the spring months of 1977–82 exhibited a TS structure.

However, our initial investigation of May 1996 MCSs for the entire United States (Parker 1999) revealed recurrent modes of linear convection other than the leading-line trailing-stratiform archetype. We observed numerous cases for which a large proportion of the stratiform precipitation existed in advance of a moving convective line (the LS mode). While previously recognized theoretically by Moncrieff (1992) and from Swiss operational data by SHH95, these systems have received relatively little study, perhaps because their complicated nature is unamenable to numerical simulation. In addition, a third mode existed in which stratiform precipitation moved (in a storm-relative sense) parallel to an MCS's convective line (this mode is hereafter called PS). The PS MCSs have apparently received even less attention to date than LS MCSs. Notably, characteristics of both the LS and PS modes are evident in the squall line archetype presented by Newton and Fankhauser (1964).

Our preliminary observations motivated a more detailed analysis of MCSs in the central United States (due to the wind profiler network and high frequency of MCSs there). The present work addresses the relatively less-studied LS and PS (in addition to TS) MCSs as a population, from which we infer their common reflectivity and environmental characteristics. In sections 2 and 3 we outline the terminology and procedures used for this work. In sections 4 and 5 we introduce in detail the three linear MCS modes and discuss their radar-observable traits. In section 6 we present the general synoptic conditions that accompanied the MCSs in this study. Thereafter, we focus on environmental wind and thermodynamic signals that varied among the LS, PS, and TS archetypes, including case study examples of an LS and PS MCS for additional insight. The aim of this paper is to document the existence and frequency of these convective modes and to outline a conceptual model for the LS and PS archetypes that is consistent with the observations from our study. By incorporating high-resolution national radar data, we were able to more fully depict mesoscale convection throughout its lifetime than were many previous researchers. Hopefully, this work will thereby shed further light on the long-standing problem of MCS organization and its predictability.

2. Terminology

Numerous interpetations of Zipser's (1982) initial definition of MCS have arisen in the past two decades. In particular, radar meteorologists have imposed reflectivity-based criteria upon the definition in order to expedite and objectify the selection of cases and compilation of populations for investigation (e.g., Geerts 1998). For the purposes of this study, we define an MCS as a convective phenomenon for which the Coriolis acceleration is of the same order as other terms in the Navier–Stokes equations. The appropriate MCS timescale is therefore f^{-1}, which is identical to that identified by Emanuel (1986) for mesoscale circulations. A typical midlatitude value for f yields an MCS timescale (τ) of approximately 3 h. Using an advective assumption, we define the length scale for this study as $L = U\tau$. An average midlatitude wind speed (U) of 10 m s^{-1} yields an MCS length scale of 100 km, identical to that suggested by Houze (1993). Only those groups of convective echoes with extents greater than 100 km and durations greater than 3 h are included in this study.

We discuss MCSs using several descriptors, among which are *linear* and *nonlinear*. Linear MCSs are those containing a *convective line,* by which is meant a contiguous or nearly contiguous chain of convective echoes that share a nearly common leading edge and move approximately in tandem, whether they are arranged in a nearly straight line or a moderately curved arc. Within the context of this study, large convecting systems with highly eccentric precipitation patterns but without convective lines are considered nonlinear MCSs. As well, we distinguish between *warm sector* (hereafter denoted as WS) and *non-warm sector* (hereafter denoted as non-WS) MCSs. Warm sector MCSs occur in the warm, moist, (typically) conditionally unstable air mass demarked by synoptic fronts, a region referred to as a warm sector in the seminal work of Bjerknes and Solberg (1922), while non-WS MCSs occur on the cold side of a synoptic-scale warm or stationary front. Finally, we have attempted in this study to refrain from use of the term *squall line* altogether due to its vagaries. When it does appear, it is to emphasize the familiarity between the present study and those of the past that, in name or in substance, specifically treated squall lines. In such circumstances, we have inferred a general meaning for squall lines similar to that advanced by Huschke (1959), to wit: "any . . . line or narrow band of active thunderstorms."

3. Data utilized and methods of analysis

The spatial domain for this study generally included the Great Plains of the United States, from about 31°–

45°N and 89°–106°W, a region known both for its frequent convective weather and its operational array of wind profilers [the National Oceanic and Atmospheric Administration (NOAA) Profiler Network, or NPN]. We cataloged and analyzed linear MCSs from the months of May 1996 and May 1997. We chose the month of May because it exhibits widespread convective activity within the NPN. In addition, May represents a period of transition between the strong baroclinic forcing of early spring and the weaker, more barotropic forcing of the summer months, such that our population should represent a spectrum of forcing types. We utilized May data from two years in order to alleviate to some extent annual biases in the data as well as to ensure that a sufficient number of cases (88) were present to allow for high confidence in the statistical results of this survey. Ultimately, the population size represented a compromise between our desire for many cases and the time-consuming nature of the radar investigation.

a. National radar base scan summaries

In order to identify and characterize the convective systems in this study, we utilized national radar composite summaries. Such composites are generated from the radar reflectivity factor (dBZ) for base scans (0.5° elevation) from the currently operational National Weather Service radars in the continental United States. The radar data composites have a time interval of 15 min, a pixel size of 2 km $\times$ 2 km, and comprise 16 levels of reflectivity factor in 5-dBZ increments (beginning with 0–5 dBZ). The composite reflectivities represent the highest instantaneous reflectivity measurement for a point at each compositing time. We chose the national radar summaries for their reasonable temporal and spatial resolution along with their ability to provide a general overview of regional radar returns. The focus of this study was the meso-β-scale (Orlanski 1975) organization and evolution of large, persistent convective systems, which were well depicted by the composite data. As the position, movement, and horizontal extent of MCSs often preclude complete sampling by one radar site, the composited data provided an advantageous depiction of storms in their entirety.

The radar data were animated using a 1-h time step over the entire study domain and a 15-min time step on the scale of each recognized MCS. Our procedure for distinguishing various modes of convection using these animations will be described in section 4. We noted each MCS's location, movement, and orientation from the radar data. We computed the system motion vector as the change in the location of the center of the leading edge of the convective line with time. We measured orientation as the mean azimuthal angle of 1) a tangent to the convective line at its centerpoint and 2) a line connecting the two endpoints of the convective line. In this study convective echoes are those with reflectivity factors greater than 40 dBZ; stratiform echoes are those

with reflectivity factors from 20–40 dBZ. These definitions correspond to the criteria used by Geerts (1998), who discovered that slight modifications to the thresholds (i.e., 15 vs 20 dBZ for the minimum stratiform echo) had little effect on MCS recognition or partitioning. We did not consider echoes less than 20 dBZ during our measurements. We also did not attempt to document or measure the movement of individual convective cells due to the limited temporal and spatial resolution of the national radar summaries.

b. National Weather Service rawinsonde observations

We selected one radiosonde observation (raob) for each MCS case in order to depict the environment within which the studied convective systems occurred. In some studies (e.g., Bluestein and Parks 1983; Bluestein and Jain 1985; Bluestein et al. 1987), an interpolation of rawinsonde soundings toward a near-storm environment was attempted. Given the coarseness of the operational rawinsonde network in the United States, however, in most of the present cases only one raob met our subjective criteria for proximity, timing, and position with respect to the eventual convective storms. Accordingly, we chose an individual sounding that best represented the preconvective air mass within which an MCS occurred and utilized it without modifications, much as was done by Rasmussen and Wilhelmson (1983) and HSD90. This technique both focuses on information available to the forecaster and helps to ensure that ongoing deep convection did not contaminate the study's sounding data. We investigated each sounding for continuity with the large-scale environment [through intercomparison with other raobs and National Centers for Environmental Prediction (NCEP) reanalyses] as was suggested by Bluestein and Parks (1983). Following HSD90, a sounding was only considered to represent the first MCS to traverse a region. We did not include subsequent convective systems (prior to another sounding time) due to the high probability that the previous convection had significantly altered the environment.

c. The NOAA Profiler Network

In order to more fully characterize the wind field near MCSs, we utilized wind profiler data from the NPN. Weber et al. (1993) detailed the manner of observation for NPN wind profilers and Barth et al. (1994) described the NOAA data processing algorithms. We combined hourly winds with corresponding surface observations to render the wind profiles used in this work. For our detailed study, we selected only wind profiles positioned in advance of an ongoing MCS. While we also investigated post-MCS wind profiles, we found that in general they offered little additional insight. We accepted a priori the processing and quality control information provided by NOAA. Accordingly, we discarded hourly data that failed any portion of the quality checks (for

either the u or v wind component). Further, we visually inspected those hourly winds that passed NOAA quality control checks for vertical and temporal continuity and compared them to neighboring profiler sites, rawinsonde observations, and NCEP reanalyses to ensure their consistency. Data that were inconsistent with other sources were removed from the study. Wilczak et al. (1995) first pointed out the widespread contamination of wind profiler data by flying birds during periods of migration across the central Great Plains. We incorporated the criteria currently used by NOAA (as given by M. Barth 1998, personal communication) to flag hourly profiler winds in this study that were contaminated by migratory birds. We compared cases that failed the contamination test with regional rawinsonde observations and NCEP reanalyses [due to the high false alarm ratio discussed by Miller et al. (1997)]. We discarded any hourly winds that failed the contamination check and were unrepresentative of the consensus wind field.

d. Diagnosis of synoptic features

In order to describe the synoptic meteorology associated with the MCSs in this study, we utilized subjectively analyzed surface data as well as NCEP gridded reanalyses (Kalnay et al. 1996). Using the methods suggested by Sanders and Doswell (1995) and Sanders (1999), we analyzed commonly available (from METAR reports and NCEP charts) surface observations at 3-h intervals prior to and during the life cycles of MCSs in this study. We noted the positions of cold, warm, and stationary fronts, drylines, surface pressure troughs, outflow boundaries, and triple points. A convective system was deemed to be associated with a surface synoptic feature if more than half of its track coincided with the position of an analyzed feature. By incorporating NCEP reanalysis data, we diagnosed the presence of low-level wind maxima (low-level jets), upper-level wind maxima (upper-tropospheric jets), and middle-tropospheric shortwave troughs and ridges (including vorticity maxima and minima). The reanalysis grids utilized for this study comprised height, wind, temperature, and humidity data at mandatory levels throughout the troposphere and stratosphere. We determined the existence of low-level jets from the wind fields at 925 and 850 hPa. The definition of low-level jet had no minimum wind speed requirement, but we required that low-level wind maxima have a southerly component in order to be considered (for consistency with previous work on low-level jets). MCSs coincident with the maxima themselves were deemed to be related to the core of the low-level jet. Those coincident with the northern extent of the low-level wind maxima (and velocity gradients found there) were deemed to be related to the terminus of the low-level jet. In addition to the initial diagnosis of attendant synoptic features, we also used the NCEP reanalyses to derive mean fields for the MCS archetypes.

e. Exclusion of cases

We observed and documented all 88 linear MCSs from our radar investigation. However, we excluded from our detailed study all cases that were non-WS. MCSs were deemed to be non-WS if 1) they were located on the cold side of a front, or 2) a strong frontal inversion existed in a nearby sounding. We discarded these cases due to their frequent lack of surface-based convective available potential energy (a problem treated by Colman 1990) as well as the ambiguity of density current dynamics and inflow layer location. While the 24 (discarded) non-WS cases composed 27% of the total MCSs documented by this study, their omission facilitated a more detailed look at WS convective systems, which are more amenable to investigation with the conventional operational datasets used. We also omitted several cases from our detailed study due to the quality of data available. Of the 64 WS cases initially cataloged from the investigation of radar data, 2 were excluded due to the absence of a rawinsonde observation that reasonably represented their environment. Additionally, we omitted two WS cases from the study due to obvious contamination of the available rawinsonde data by the presence of precipitation. One case, which appeared to represent the air mass within which an MCS occurred, was omitted due to a lack of conditional instability. It is possible that modification of the sounding occurred at a later time, such as Trier and Parsons (1993) found in a case study. It is also possible that this case belongs to the class discussed by Colman (1990), wherein symmetric instability may be responsible for the dominant mode of overturning. In either case, the treatment of such soundings is beyond the scope of this investigation. In summary, of the 88 initial MCSs (of which 85 were classifiable) 64 occurred within a warm sector. Five warm sector cases were eliminated due to data concerns, yielding 59 good quality WS MCSs (of which 57 were classifiable).

No archetype was especially depleted by the omissions; approximately two-thirds of the initial cases were retained for each linear MCS mode (65% of TS cases, 71% of both LS and PS cases). While some wind profiler data failed NOAA quality control checks, 60% of the hourly wind profiles passed all tests and were utilized. Reassuringly, none of the three MCS archetypes lost a disproportionate number of wind profiler observations in the quality control procedure. The LS and PS MCSs each accounted for approximately 20% of the total cases, the retained cases (i.e., not omitted), and the wind profiler observations. The TS MCSs accounted for approximately 55% of each category, while unclassifiable cases represented the approximately 5% remaining. It appears that the omission of non-WS cases and bad observations did not preferentially affect any one subset of MCSs in this study. This gives us some confidence that we did not introduce a large bias into the study by removing data.

Linear MCS archetypes

Initiation Development Maturity

a. **TS**
Trailing stratiform

b. **LS**
Leading stratiform

c. **PS**
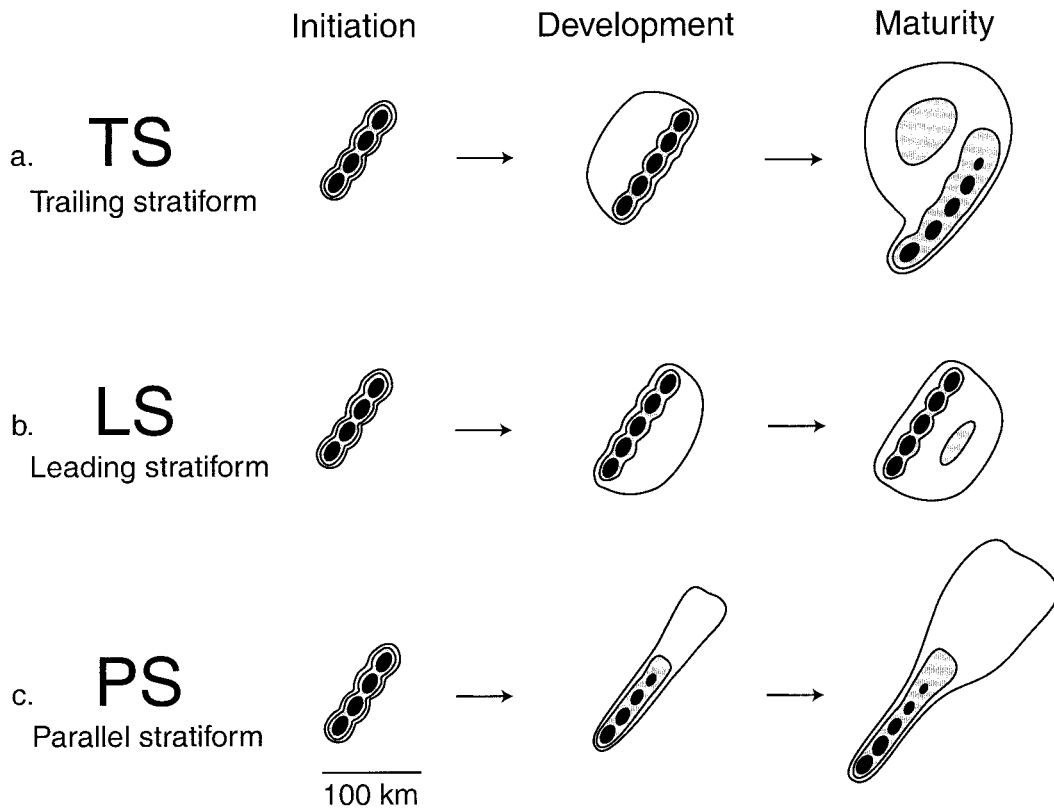Parallel stratiform

100 km

FIG. 4. Schematic reflectivity drawing of idealized life cycles for three linear MCS archetypes: (a) TS, (b) LS, and (c) PS. Approximate time intervals between phases: for TS 3–4 h; for LS 2–3 h; for PS 2–3 h. Levels of shading roughly correspond to 20, 40, and 50 dBZ.

4. Three modes of linear mesoscale convective system

The 88 linear MCSs from May 1996 and May 1997 were classified into three basic categories (Fig. 4). Several assumptions are implicit in the taxonomy presented here. First, we only cataloged linear MCSs in this study. The following taxonomy makes no attempt to describe or account for nonlinear MCSs. Second, all of the cases classified herein (and on which the definitions are based) met our definition of MCS. While the organizational modes depicted herein may be reflected in convection on smaller scales, the results of the present study are focused on systems at least 100 km in extent and 3 h in duration. Third, we observed all the MCSs in this study using national radar composites. Accordingly, the taxonomy presented here is based solely upon the meso-β-scale radar reflectivity structures of the documented MCSs, not upon their dynamics, velocity fields, or other observable properties. While we hypothesize that the three linear MCS modes may have distinct kinematic structures, we are as yet unable to evaluate this hypothesis owing to the lack of suitable, detailed obser-

vations. We set forth our taxonomy of radar structures as a basis for such desirable future investigations.

In order to classify the linear MCSs in this study, we animated and carefully observed radar data on the scale of each system. If an MCS bore great likeness to any one of the three archetypes, we classified it as such. To classify cases with more ambiguous combinations of archetypal qualities, we considered the relative extent of stratiform precipitation ahead of (i.e., LS), behind (i.e., TS), and parallel to (i.e., PS) the convective line; the stratiform region's storm-relative displacement vector; and the predominance of an organizational mode throughout the MCS's lifetime. An MCS that initially exhibited LS structure for 6 h and then evolved toward TS structure for 2 h (before decaying) was classified as LS, for example. Cases from the radar study were only *unclassifiable* if 1) they bore no resemblance to any of the three archetypes presented below, or 2) they evolved among archetypes with no clear and dominant mode of organization, or 3) a preexistent meso-α-scale stratiform precipitation region obscured or made unclear the amount of stratiform precipitation actually produced by

the MCS itself (i.e., an embedded convective line), or 4) no appreciable stratiform precipitation was evident in the 2-km radar data. We reemphasize the importance of animating the radar data in the above procedure: it was not the instantaneous structure but the persistent, predominant organizational mode of an MCS that we considered. By way of analogy to HSD90, we believe that all of the classified cases are either "strongly" (i.e., exemplifying the archetype) or "moderately" (i.e., resembling the chosen archetype notably more than the other archetypes) classifiable, though these designations (here) are subjective. The existence of relatively few unclassifiable cases (3 of 88 total) suggests that within the spectrum of linear MCSs, observable similarities to one of the three presented archetypes are common.

a. Trailing stratiform

The TS MCS archetype (Fig. 4a) was described by HSD90 and we have not departed from the definition that they presented. The pertinent aspects of the definition advanced by HSD90 include a convective line, "convex toward the leading edge," with "a series of intense reflectivity cells solidly connected by echo of more moderate intensity." The line has a "very strong reflectivity gradient at [the] leading edge (i.e. gradient much stronger at [the] leading edge than [the] back edge of the convective region)," and a large trailing stratiform precipitation region, often exhibiting a "secondary maximum of reflectivity separated from the convective line by a narrow channel of lower reflectivity" (the *transition zone*). It is relevant to note that the TS archetype depicted by HSD90 exhibited very little leading stratiform precipitation (e.g., Fig 1). Three examples of TS MCSs in our study are shown in Fig. 5.

b. Leading stratiform

We define linear MCSs whose stratiform precipitation is predominantly located in advance of a convective line (i.e., in the area toward which the MCS propagates) as *convective lines with leading stratiform precipitation* (or simply LS, Fig. 4b). This archetype was apparently first recognized in Swiss MCSs by SHH95, although it also bears some resemblance to the squall line model introduced by Newton and Fankhauser (1964). In the extreme, members of this class exhibit a convective line preceded by a transition zone and secondary swath of stratiform precipitation with a reflectivity maximum (Fig. 6a). More frequently, LS MCSs exhibit moderate regions of leading stratiform precipitation without transition zones and secondary bands (Figs. 6b–d). The tendency of an MCS to generate predominantly preline precipitation is a criterion for LS classification even if postline precipitation is present. Cases with extensive preline and postline precipitation obviously represent a transition between the two extreme archetypes. We typically classified these as LS based upon their greater

qualitative similarity to the LS extreme than the TS extreme (since the preline reflectivity gradient is not significantly different from the postline gradient the TS archetype, as defined by HSD90, is not appropriate).

c. Parallel stratiform

We deem a linear MCS to have a *convective line with parallel stratiform precipitation* (or simply PS) if most or all of the stratiform precipitation region associated with the convective line moves parallel to the line itself (in a storm-relative framework) and to the left of the line's motion vector throughout its life cycle (Fig. 4c). Very little stratiform precipitation surrounds the convective lines of PS cases (Fig. 7). More formally, the reflectivity gradient is relatively large on both sides of the convective line. The stratiform regions' movements (as determined from animations) in PS cases generally deviate less than 30° from the convective lines' (azimuthal) orientations. In some cases, PS convective lines backbuild to the right of their motion vectors. Such behavior may be accompanied by the general decay of convective cells to the left of a line's motion vector, yielding a progressively larger region of lower reflectivity echoes to the left of and parallel to the convective line. In other cases, PS convective lines do not appear to backbuild substantially. Rather, a location of persistent deep convection appears to give rise to the PS echoes via line-parallel advection. Probably both processes are at work to some degree in most PS MCSs.

5. Radar-observed traits of the MCS population

a. Distributions of MCS cases

While the oft-studied TS archetype is the most prevalent of the three classes (accounting for 58% of the 88 total linear MCSs), a primary new result of this study is that sizeable populations of the LS and PS modes exist. Of the 88 cases examined in the study domain during May 1996 and May 1997, LS and PS cases each composed 19% of the total linear MCS population (Table 1). On average TS cases met the MCS length and reflectivity criteria for nearly twice as long (12.2 h) as LS and PS cases (6.5 and 6.3 h, respectively), as suggested by the growth-stage intervals in Fig. 4. As well, they were the swiftest of the three classes (Table 1). Therefore, TS cases traversed far greater distances than did other members of the linear MCS spectrum. All three archetypes most frequently were oriented northeast–southwest, roughly along 60° azimuth (Fig. 8), a result similar to that found by Geerts (1998) for southeastern U.S. MCSs. The TS class had the strongest northeast–southwest-orientation mode, in part due to TS MCSs' frequent relationship to synoptic cold fronts in this study (not shown), which typically had a more consistent azimuthal orientation than did warm or stationary fronts and other linear boundaries. Each class, on average,

a) 0700 UTC, 8 May 1997

b) 0200 UTC, 23 May 1997
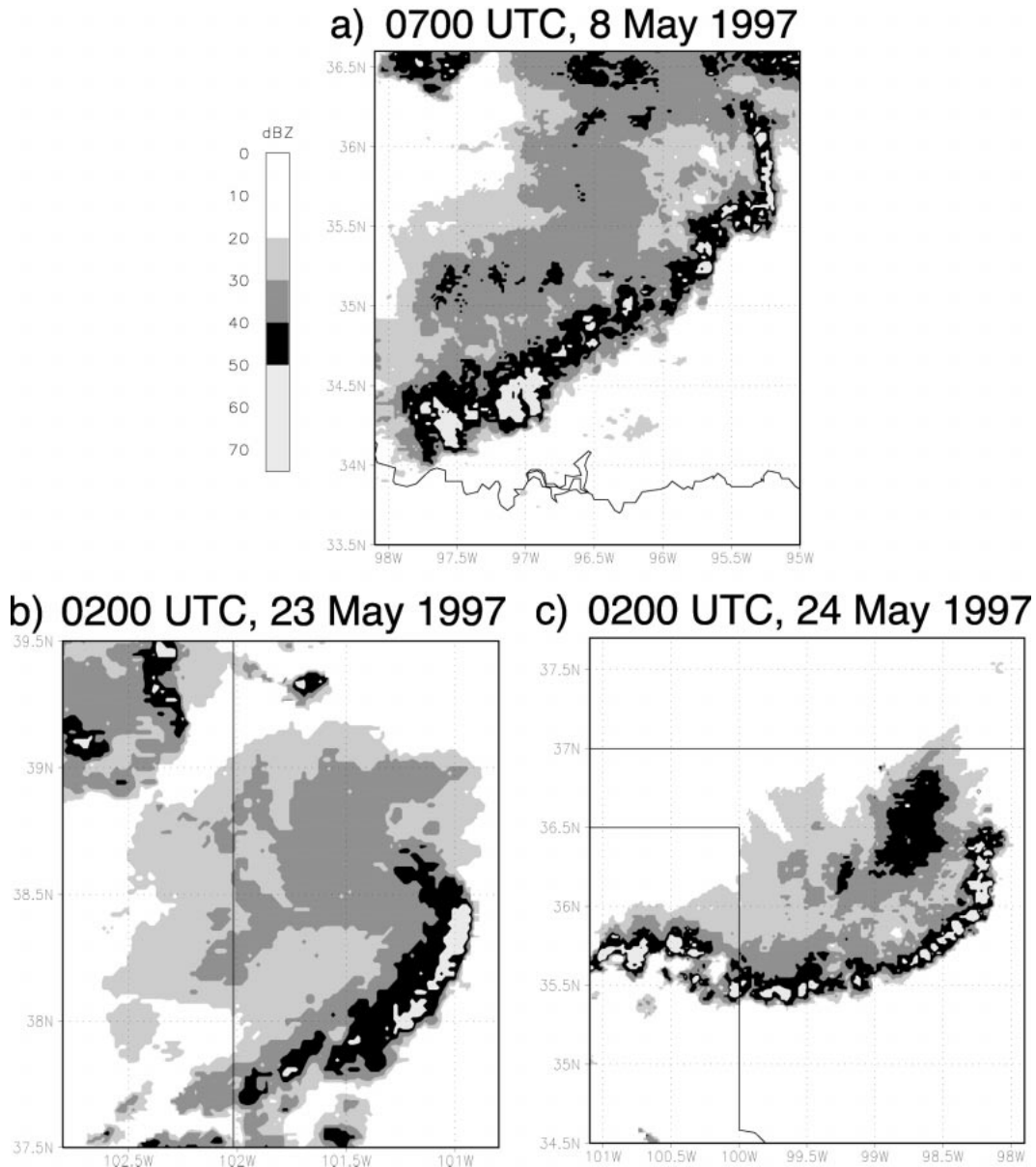
c) 0200 UTC, 24 May 1997

FIG. 5. Radar reflectivity—examples for TS archetype: (a) 0700 UTC 8 May 1997, (b) 0200 UTC 23 May 1997, and (c) 0200 UTC 24 May 1997.

moved from roughly the west or west-northwest (Table 1).

b. Evolution among archetypes

As may be expected, linear MCSs can and do frequently evolve among archetypes between their initiation and decay. As detailed above, the cases in this study, when evolving, were classified based upon their predominant organizational modes. Not surprisingly (given the total MCS distribution), nearly half of all linear MCSs initially possessed TS characteristics (Fig. 9). Relatively few MCSs that began as TS evolved into the other modes. Conversely, 30% of all cases that began as LS evolved to TS, and 58% of all cases that began as PS evolved to TS. These results may account for the large number of TS cases documented by HSD90; that is, a great deal of linear MCSs appear to have TS characteristics at some point in their lifetimes, even if their initial organization is distinctly non-TS. It may be that, in time, convective lines begin to accelerate forward, such that TS rain is favored in their later stages. This hypothesis derives in part from the numerical results of Crook and Moncrieff (1988), who found that simulated convective lines evolved in time from overturning updrafts to jump updraft dominance. Notably, few MCSs
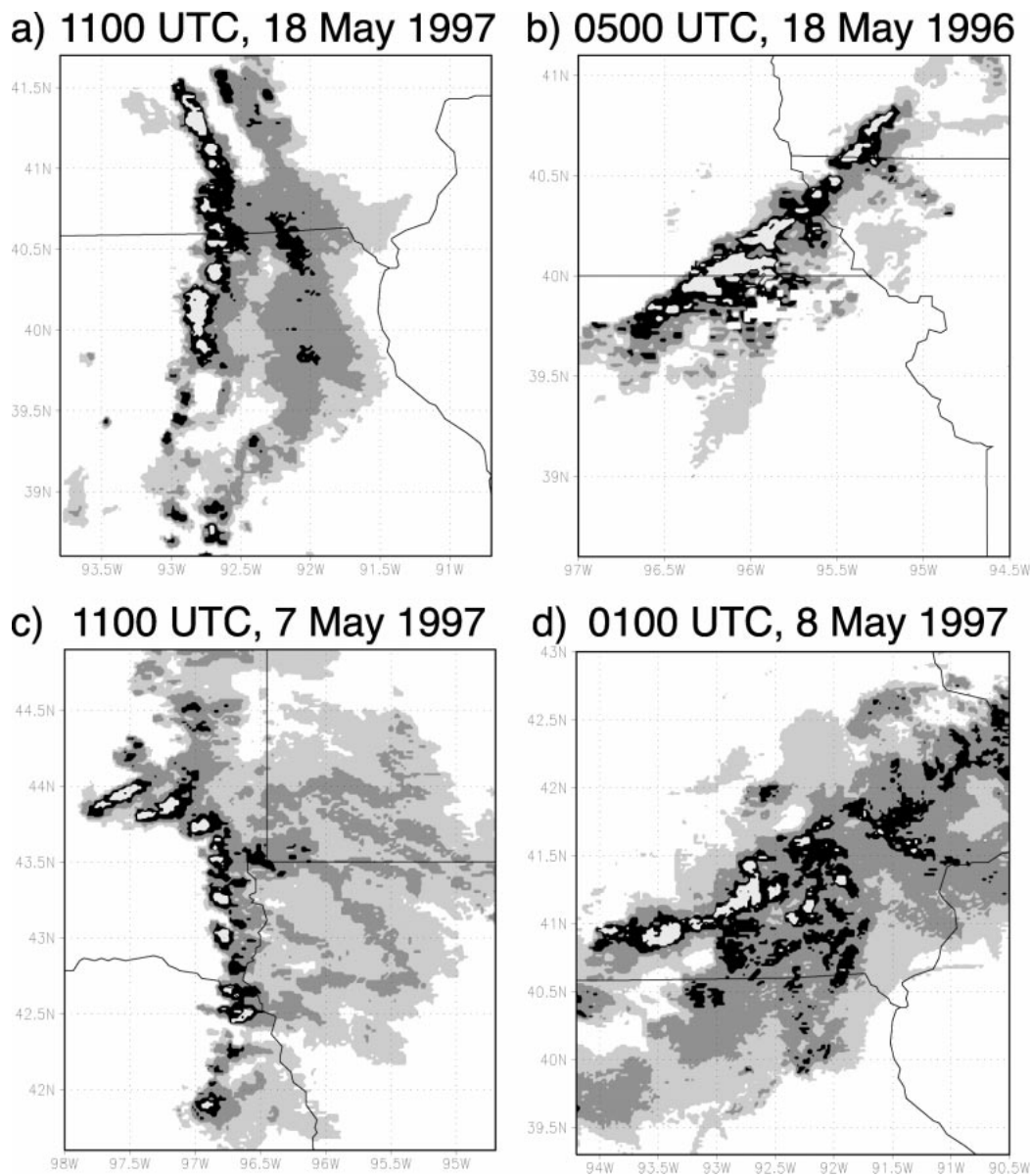
FIG. 6. Radar reflectivity—examples for LS archetype: (a) 1100 UTC 18 May 1997, (b) 0500 UTC 18 May 1996, (c) 1100 UTC 7 May 1997, and (d) 0100 UTC 8 May 1997. Reflectivities shaded as in Fig. 5.

evolved toward the PS archetype. If, as suggested by the case study in section 8, a unique juxtaposition of low-level convergence boundaries and upper-level winds is important to some PS cases, it may be that such arrangements are not generally produced during ongoing convective events.

c. Diurnal variability

Nocturnal maxima have been established for thunderstorms (Wallace 1975), MCCs (Maddox 1980), and "mesoscale precipitation systems" (HSD90) in the central plains. Our study confirms this nocturnal maximum for 64 linear WS MCSs (Fig. 10). The dominant signal

in the total curve for linear MCSs is centered at 2200 central daylight saving time (CDT, or 0300 UTC). This maximum agrees well with the finding of HSD90 that mesoscale precipitation systems with "extremely large stratiform areas" were maximized between 2200 and 0400 CDT (0300 and 0900 UTC). Hilgendorf and Johnson (1998) pointed out that an MCS's maximum areal extent typically occurs later than the midpoint in its lifetime. As the times represented in Fig. 10 are approximate midpoints in MCS lifetimes, the nocturnal maximum may therefore be slightly displaced toward an earlier hour than that observed by HSD90, who used the time of "maximum stratiform echo." The majority of TS cases occurred between 2000 and 0200 CDT
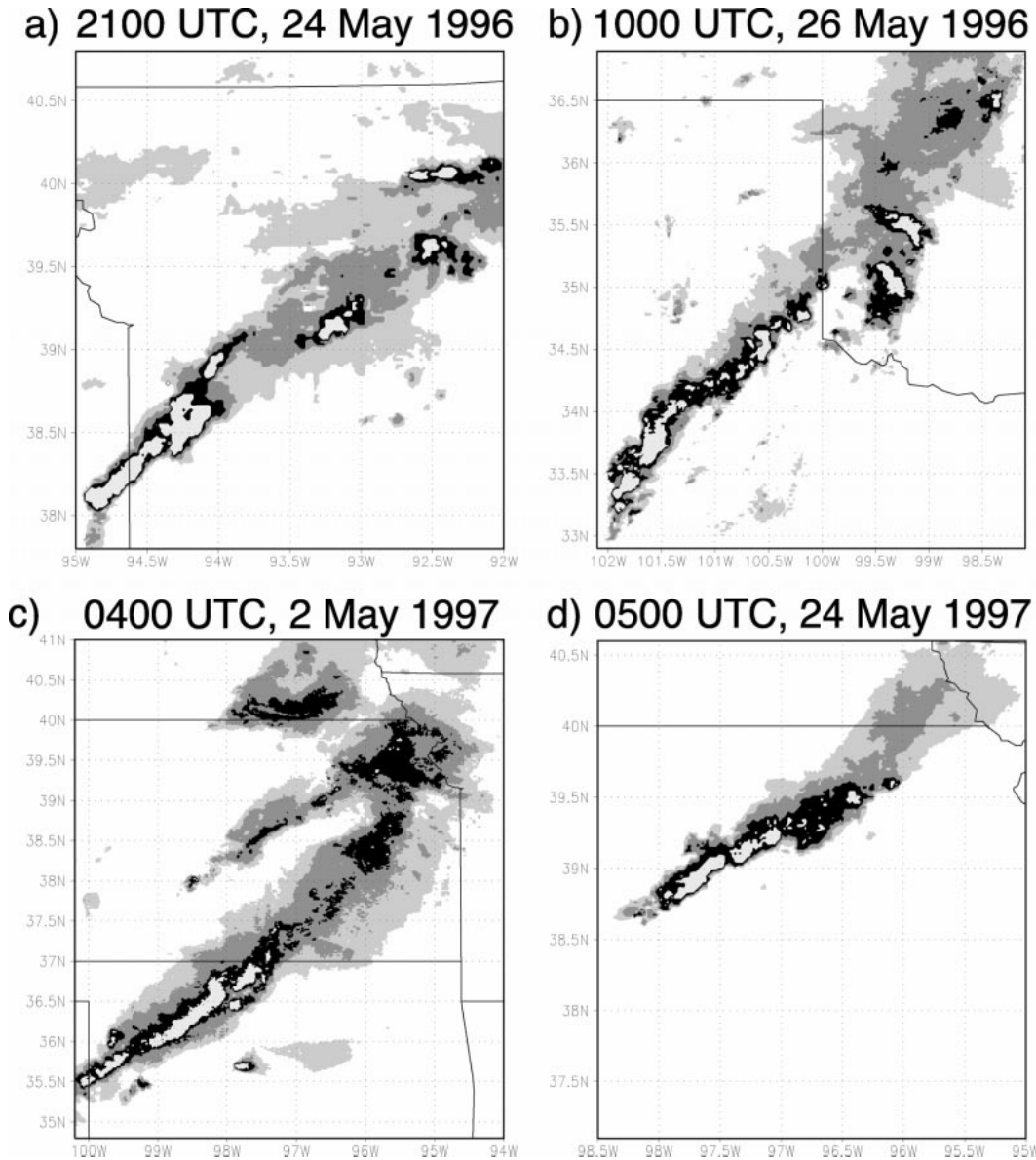
FIG. 7. Radar reflectivity—examples for PS archetype: (a) 2100 UTC 24 May 1996, (b) 1000 UTC 26 May 1996, (c) 0400 UTC 2 May 1997, and (d) 0500 UTC 24 May 1997. Reflectivities shaded as in Fig. 5.

TABLE 1. Summary of fundamental information for TS, LS, PS, and unclassifiable linear MCSs. Indicated duration is the length of time that MCS criteria were met. Mean duration, speed, and heading were not calculated for unclassifiable cases.

	TS	LS	PS	Un-class.
No. of total cases (88)	51	17	17	3
No. of warm sector cases (64)	34	13	15	2
Mean duration (h)	12.2	6.5	6.3	n/a
Mean speed (m s^{-1})	13.0	7.1	11.4	n/a
Mean heading (azimuth)	275	294	289	n/a

(0100 and 0700 UTC), with a smaller mode in PS cases between 1700 and 0000 CDT (2200 and 0500 UTC) and LS cases between 1800 and 0000 CDT (2300 and 0500 UTC). In addition, a secondary mode existed near local sunrise ($\approx$0600 CDT, or 1100 UTC). While this secondary maximum was relatively small for TS MCSs (with respect to the amplitude of the archetype's curve), it appeared to be the dominant mode for LS MCSs. Geerts (1998) noted a similar secondary maximum in MCSs of the southeastern United States. It may be that by utilizing regional radar data a secondary maximum that was unapparent from satellite imagery has been revealed. The reasons for this near-sunrise mode are not fully understood at this time. One hypothesis, advanced
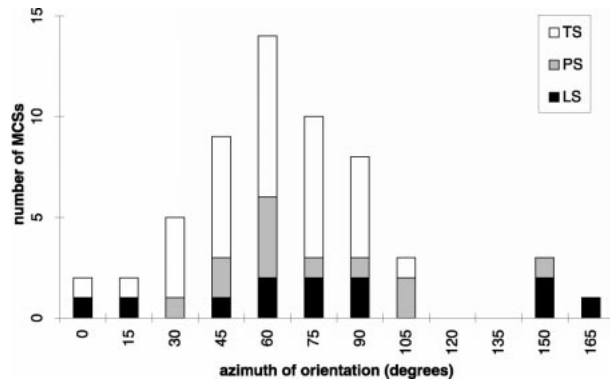
FIG. 8. Histogram of warm sector linear MCSs' azimuth of orientation by archetype (0° and 180° correspond to a convective line whose tangent is N–S, 90° corresponds to a convective line whose tangent is E–W). Abscissa values represent 15° bins centered at the given value. Orientations depicted are lifetime means for each MCS. Note that a convective line's direction of motion is not uniquely determined by its orientation.

by Gray and Jacobson (1977) for tropical deep cumulus clouds, relates enhanced near-sunrise upward motions to solenoidal circulations forced by the difference in nocturnal radiational cooling between cloudy and clear areas.

6. Synoptic environment of MCSs during the study

In order to compare episodes of linear MCS prevalence to episodes of their absence, we constructed mean fields for periods deemed to be *active* and *inactive*. A period was active if it 1) produced at least one MCS per day during a contiguous series of two or more days, or 2) produced at least two MCSs during an individual day. Based upon our partitioning, 85 of the 88 observed cases occurred during active periods. Active–inactive difference fields were constructed from NCEP reanalyses for the 64 linear WS MCSs in this study. The general synoptic patterns associated with each class of linear MCS were roughly the same, such that only the gross population traits are depicted here.

The May 1996 and May 1997 data are consistent with the prevalant idea that MCS activity increases in the presence of an approaching short wave trough and/or wave cyclone (Kane et al. 1987). During active periods, average mean sea level pressures were lower across the entire central plains due to the traversal of surface cyclones (Fig. 11a). The strongest signal is the tendency for a low pressure center in southwestern Kansas during active regimes. We attribute this result in large part to a persistent high plains low pressure feature during May 1996. In addition, however, the west-to-east tracks of the cyclones that crossed the study domain originated mainly in the high plains, a tendency that strengthened the mean perturbation in southwestern Kansas.

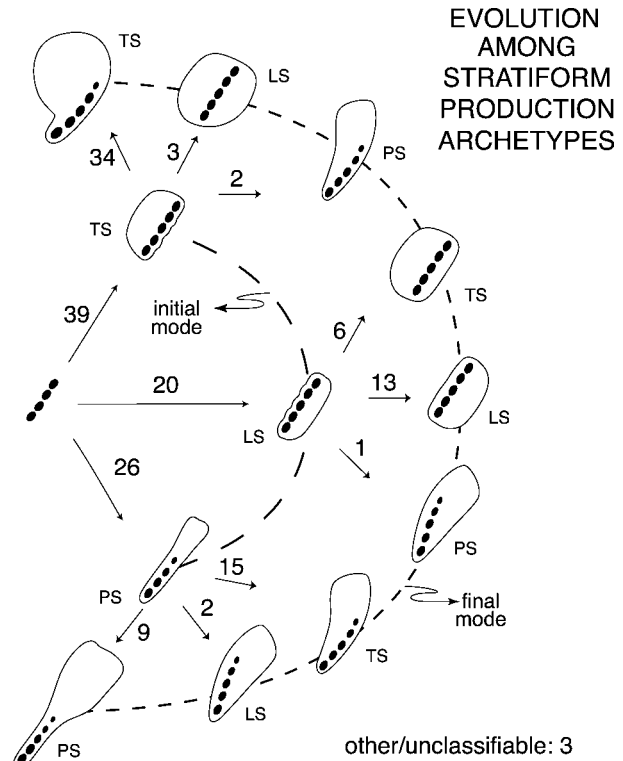The mean surface cyclone was well related to lowered

FIG. 9. Illustration of evolutionary pathways for MCSs in this study. Labels along each pathway denote the initial and final modes of stratiform precipitation production. The total number of cases following each step is indicated. Idealized composite positions of convective elements and stratiform precipitation are depicted schematically along each pathway. Note: some pairs of evolutionary pathways (e.g., TS → PS and PS → TS) resulted in generally similar reflectivity patterns. As discussed in the text, MCSs were classified based upon their predominant organizational mode, which could be either their initial or final organization.
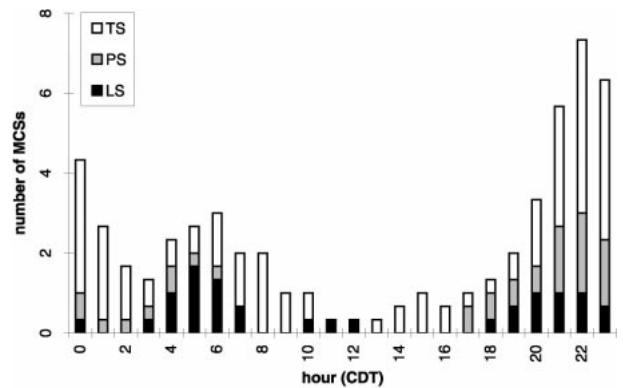

FIG. 10. Histogram of diurnal distribution for warm sector linear MCSs. Times depicted are centerpoints of each MCS lifetime. Times are (local) CDT: CDT = UTC − 0500. Values are smoothed using a 3-hourly running mean.

a) MSLP (1 hPa)   500 hPa z (20 dam)
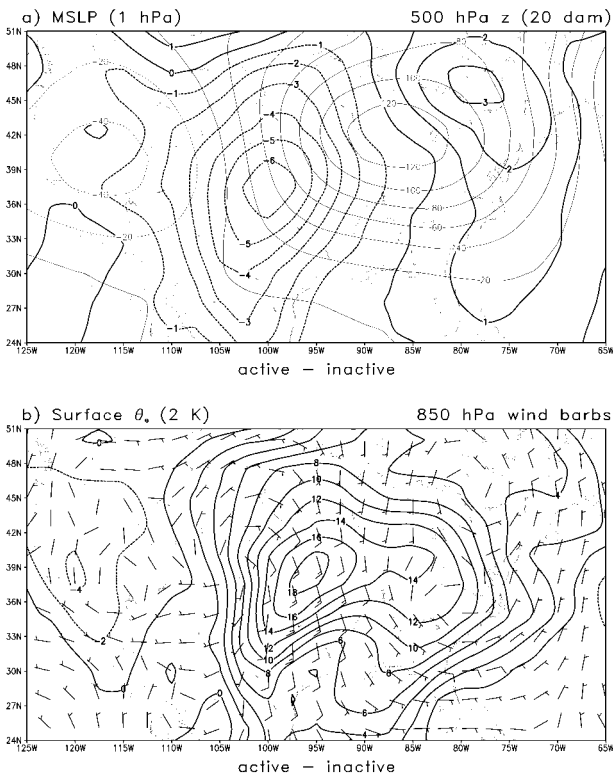

b) Surface θ_e (2 K)   850 hPa wind barbs

FIG. 11. NCEP reanalysis mean difference fields: active–inactive periods. (a) Surface pressure reduced to mean sea level (hPa, heavy contours; dashed, negative) and 500-hPa geopotential height (dam, light contours; dashed, negative). (b) Surface equivalent potential temperature (K, contours; dashed, negative) and 850-hPa wind barbs: barb = 5 m s^{-1}, half barb = 2.5 m s^{-1}.

TABLE 2. Distribution of synoptic features related to the 88 studied cases. *Boundary intersection* (int.) MCSs occurred at or near the colocation of two features (B–F). Therefore, A + B + C + D + E + F + N − int. = 88.

Code	Synoptic feature	No. of cases	% cases
A	Non–warm sector	24	27
B	Warm or stationary front	24	27
C	Surface pressure trough	21	24
D	Cold front	19	22
E	Outflow boundary	8	9
F	Dryline	7	8
N	No apparent surface feature	1	1
int.	Boundary intersections	16	18
G	Low-level jet core	30	34
H	Low-level jet terminus	24	27
X	No low-level jet feature present	34	39

warm, moist, increasingly buoyant air from the Gulf of Mexico region. This enhanced southerly flow is consistent with the increased presence of low-level jets during active periods. Indeed, 61% of the linear MCSs in this study were associated with either the core or terminus of a low-level jet (Table 2). The presence of a linear trigger is also apparently important to linear warm-sector MCSs. Sixty-three of the 64 WS cases occurred near a linear synoptic boundary. Linear WS MCSs were most frequently associated with warm or stationary fronts, closely followed by surface pressure troughs and cold fronts (Table 2). These results confirm those of prior studies (e.g., Bluestein and Jain 1985; Purdom 1986; Bluestein et al. 1987), underscoring the importance of lower-tropospheric convergence for organized convection.

7. Physical description of linear MCS archetypes and their environments

While all 88 MCSs in the study were classified, the average fields presented in this section represent only the 57 classifiable, good quality, warm-sector MCSs not omitted for the reasons described in section 3. The means depicted hereafter include 33 TS MCSs, 12 LS MCSs, and 12 PS MCSs.

a. Wind fields and their relationship to stratiform precipitation distribution

For each linear MCS we selected nearby NPN wind profiles from three times at which the reflectivity structure best resembled the case's predominant organizational archetype. These profiles were then composited to produce mean wind fields for each linear MCS mode. The TS cases' mean line-perpendicular storm-relative wind components, as constructed from the profiler data, were significantly different from those of the LS and PS classes. The TS class mean exhibited negative line-perpendicular storm-relative winds at every level (Fig. 12). Above 2 km, TS cases exhibited significantly larger
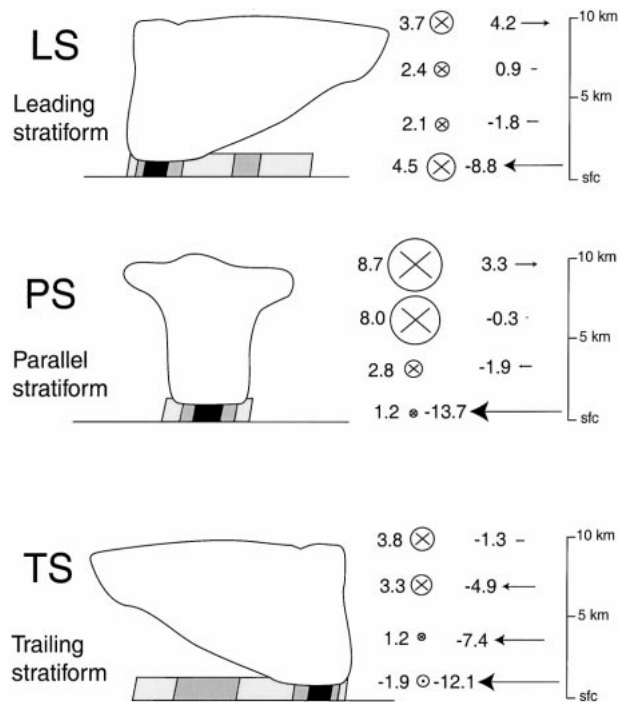
geopotential heights in the middle and upper troposphere over the western United States due to approaching short-wave troughs (Fig. 11a). In association with the enhanced troughing, stronger upper-tropospheric cyclonic vorticity advection occurred over the study domain during active periods (not shown), implying quasigeostrophic ascent. On average, linear MCSs occurred in the right entrance region of an upper-tropospheric jet streak (not shown), a region frequently associated with upper-level divergence and upward motion as described by Uccellini and Johnson (1979). In addition, Blanchard et al. (1998) discussed the possibility that weak inertial stability, such as on the equatorward side of a westerly jet, may contribute to the upscale growth of convective cells into MCSs. The strengthened ridge over the central and eastern United States during active periods (Fig. 11a) is consistent with a warm air mass in place over the plains and Midwest during the MCS episodes. During active regimes, a tongue of high-θ_e air extended into the central plains from south-central Texas (Fig. 11b), generally in association with increased lower-tropospheric warm air advection (not shown). During active periods stronger southerly flow tended to prevail at low levels across the southern two-thirds of the study domain (Fig. 11b), which suggests the northward flow of

FIG. 12. Vertical profiles of layer-mean storm-relative pre-MCS winds for linear MCS classes. Wind vectors depicted as line-parallel ($\otimes$) and line-perpendicular ($\rightarrow$) components in m s^{-1}. Layers depicted are 0–1, 2–4, 5–8, and 9–10 km. Typical base scan radar reflectivity patterns (shading) and hypothetical cloud outlines are drawn schematically for reference. MCSs' leading edges are to the right.

TABLE 3. Summary of statistically significant (at 0.05) thermodynamic rawinsonde variables. Units: CAPE, J kg^{-1}; LCL and CCL, hPa; all temperatures and LI, K; PW, cm. Also, T_v is the surface virtual temperature; $T_{v_{dd}}$ is the surface virtual temperature of minimum θ_w downdraft (as described in text); T_{vT_w} is the surface virtual temperature when cooled to saturation.

Field	LS	PS	TS
CAPE	1009	813	1605
LCL	811	765	831
CCL	735	686	778
LI	−3.5	−2.2	−5.4
$T_{v_{dd}} - T_v$	−0.8	−2.1	−4.8
$T_{v_{dd}} - T_{vT_w}$	5.3	4.1	0.7
PW	3.27	2.43	3.35

average rear-to-front component of the storm-relative flow aloft, which may help to explain the forward advection of hydrometeors. The upper-tropospheric shear for LS cases was not dramatically different from that observed in PS and TS MCSs, such that shear aloft may not (as suggested by Grady and Verlinde 1997) universally explain preline precipitation. The 5–8- and 3–10-km mean line-perpendicular storm-relative winds were by far the most statistically significant differentiators among the three classes in this study, suggesting that the middle- and upper-tropospheric storm-relative flow field is of primary importance in determining the organizational mode of linear mesoscale convection. Rasmussen and Straka (1998) similarly concluded that the strength of storm-relative winds is well correlated with the evolution of supercell thunderstorms into low, classic, and high precipitation structures. Some component of the storm-relative winds is due to storm motion, which was also significantly different (at 0.05) among the three classes (cf. Table 1). However, ground-relative winds (both u and v components) were also significant at the 0.05 level in the 0–6-, 3–10-, 5–8-, and 9–10-km layers.

b. Durations of linear MCS classes

The mean TS MCS lasted nearly twice as long as LS and PS MCSs. This appears to be correlated with the stability of the air masses into which TS cases propagated. The mean convective available potential energy (CAPE), lifting condensation level (LCL), convective condensation level (CCL), and lifted index (LI) imply that TS MCSs occurred in air masses with the most conditional instability, while PS cases occurred in air masses with the least (Table 3). As well, the lower-tropospheric storm-relative flow (Fig. 12) suggests that inflow toward LS cases (in the mean) passed through the stratiform precipitation region, which was not the case for either the PS or TS classes. Crook and Moncrieff (1988) discovered similar behavior in a modeled convective line and noted several observational examples (e.g., Tripoli 1987). A fundamental question arises regarding the longevity of LS cases, namely their per-

rearward storm-relative winds than those observed for the LS and PS classes. This result is consistent with rearward advection of hydrometeors by the mean flow, which has been argued to explain trailing stratiform precipitation regions (e.g., Rutledge 1986; Rutledge and Houze 1987; Houze et al. 1989; Biggerstaff and Houze 1991). In contrast, the LS and PS classes were nearly indistinguishable from one another in most of the line-perpendicular fields, exhibiting weak middle-tropospheric storm-relative winds and modest rear-to-front storm-relative winds at upper levels (Fig. 12). The notable exception was the 0–1-km layer, in which the magnitude of line-perpendicular flow for the PS cases was, on average, greater than that of the TS cases.

The lower-tropospheric line-perpendicular winds near PS cases were quite strong within a shallow layer. Above 2 km, PS MCSs exhibited deep line-parallel storm-relative flow, such that the middle-tropospheric advection of hydrometeors was largely along the line. In the 5–8-km layer, in which Rutledge and Houze (1987) found bulk transport of MCS hydrometeors to be focused, PS cases exhibited almost purely line-parallel storm-relative winds. The line-perpendicular storm-relative winds attending LS cases were not remarkably distinct from those in PS cases, although the line-parallel winds were much weaker. Thus, in LS cases there was a greater

sistence despite inflow of evaporatively cooled preline air into convective towers. Perhaps inflow air cooled to its wet-bulb temperature was still positively buoyant and therefore fueled the LS updraft towers in some MCSs. This could be particularly appropriate in the cases where inflow air is nearly saturated prior to entering the LS precipitation. An MCS from 18 May 1997, discussed in section 8, may have been maintained by lower-tropospheric inflow of buoyant air into the rear of the convective line. This scenario is not, however, depicted in the mean post-MCS vertical wind profiles (not shown) and may, therefore, be somewhat anomalous. Fankhauser et al. (1992) observed quasi-supercellular characteristics in an LS case, which might contribute to a line's longevity. However, parameters used to predict supercellular convection (e.g., storm-relative helicity and bulk Richardson number) were not statistically significant in the present study. In addition, supercellular lines are generally regarded as rare (Rotunno et al. 1988). It may be that a variety of LS modes exist, each of which is sustained in a unique way. As PS cases do not contaminate their own inflow, their persistence is much less mysterious.

Since the strength of cold thunderstorm outflows may be significant to the sustenance of line convection (Rotunno et al. 1988), we also considered the possibility that cold pool temperature perturbations varied among MCS classes. We utilized idealized cold pool calculations from rawinsonde data to estimate the ability of MCS environments to support cold surface outflows. In doing so, we considered negatively buoyant downdrafts from a sounding's level of minimum wet-bulb potential temperature (θ_w). Parcels from this level can, via evaporative and sublimative cooling during descent, produce the coldest surface outflow. On average in this study, the level of minimum θ_w occurred near 650 hPa. We computed the surface virtual temperature of such downdraft parcels ($T_{v_{dd}}$) assuming pseudoadiabatic descent through the cloud layer, then adiabatic descent (for simplicity) below cloud base. We then compared $T_{v_{dd}}$ to the environment's surface virtual temperature (T_v) and to the virtual temperature of the surface air mass when cooled to saturation ($T_{v_{Tw}}$). Both idealized downdraft temperature perturbations ($T_{v_{dd}} - T_v$ and $T_{v_{dd}} - T_{v_{Tw}}$) were significantly different (at the 0.05 level) among the three linear MCS types. For both scenarios, the mean TS environment could produce the strongest surface cold pool temperature perturbation (Table 3). The mean TS case also had higher precipitable water (PW) and a lower LCL and CCL than did the means of the other two classes, implying a greater possible precipitation load and a lower cloud base. This might have decreased the temperature of middle-tropospheric downdraft parcels by both increasing the integrated cloud in an atmospheric column (yielding more hydrometeors for evaporation and melting) and decreasing the distance of adiabatic descent for (idealized) downdraft parcels below cloud base.

Despite their possibly weaker cold pools, PS cases should have encountered relatively uninterrupted buoyant inflowing air on a continual basis (as did TS MCSs). It is therefore somewhat surprising that PS MCSs were not, on average, longer lived than LS MCSs. Schmidt and Cotton (1990), Nicholls et al. (1991), and Mapes (1993) have discussed the gravity waves that attend mesoscale regions of convection. Mapes (1993) showed that gravity waves forced by the heating profile in MCS stratiform regions (the $l = 2$ mode), when commingled with the signal of convective heating (the $l = 1$ mode), can condition the surrounding atmosphere for further convection, making MCSs "gregarious." It is unclear for PS MCSs to what degree these gravity wave modes might act in concert, as the stratiform and convective regions are laterally displaced from one another. Perhaps the PS arrangement of precipitation is less favorable for self-sustenance due to gravity wave dynamics, which would explain in part their modest durations. Therefore, the differing lifetimes among the three MCS classes may be governed to some extent by environmental stability, the presence or absence of rainfall into inflowing airstreams, the strength of surface cold pools, and the distribution of gravity wave energy from convective and stratiform heating.

8. Case studies

a. 18 May 1997: Leading stratiform

During the morning hours of 18 May 1997, an intense LS MCS traveled eastward along the Iowa–Missouri border (Fig. 13). Throughout its lifetime of approximately 7 h, the MCS exhibited rapid east-northeastward motion (at 8–14 m s^{-1}), while producing a region of stratiform rain entirely forward of its convective line.

As a preexistent MCS moved eastward and decayed over Missouri between 0300 and 0600 UTC on 18 May, it left an outflow boundary (Fig. 14). By the time that early convection (associated with the 18 May 1997 LS MCS) developed, a pocket of enhanced lower-tropospheric (i.e., 925–850 hPa) equivalent potential temperature (θ_e) had moved northeastward and, according to the NCEP reanalysis data, was collocated with the baroclinic zone over western Missouri at 0600 UTC (not shown). Regional wind profiler data revealed a southerly low-level jet at 1 km above mean sea level (MSL) over east-central Kansas (Fig. 15). The movement of an 850-hPa height minimum toward the upper Mississippi Valley gradually created a south-southeastward height gradient across the central plains, in response to which the lower-tropospheric winds became increasingly westerly. The low-level jet was well established at Lathrop, Missouri (LTH), by 0900 UTC (Fig. 16).

The first convective echoes associated with the 18 May 1997 MCS developed over northwestern Missouri at 0700 UTC (not shown). It is possible that as the strong low-level jet became increasingly westerly, isentropic
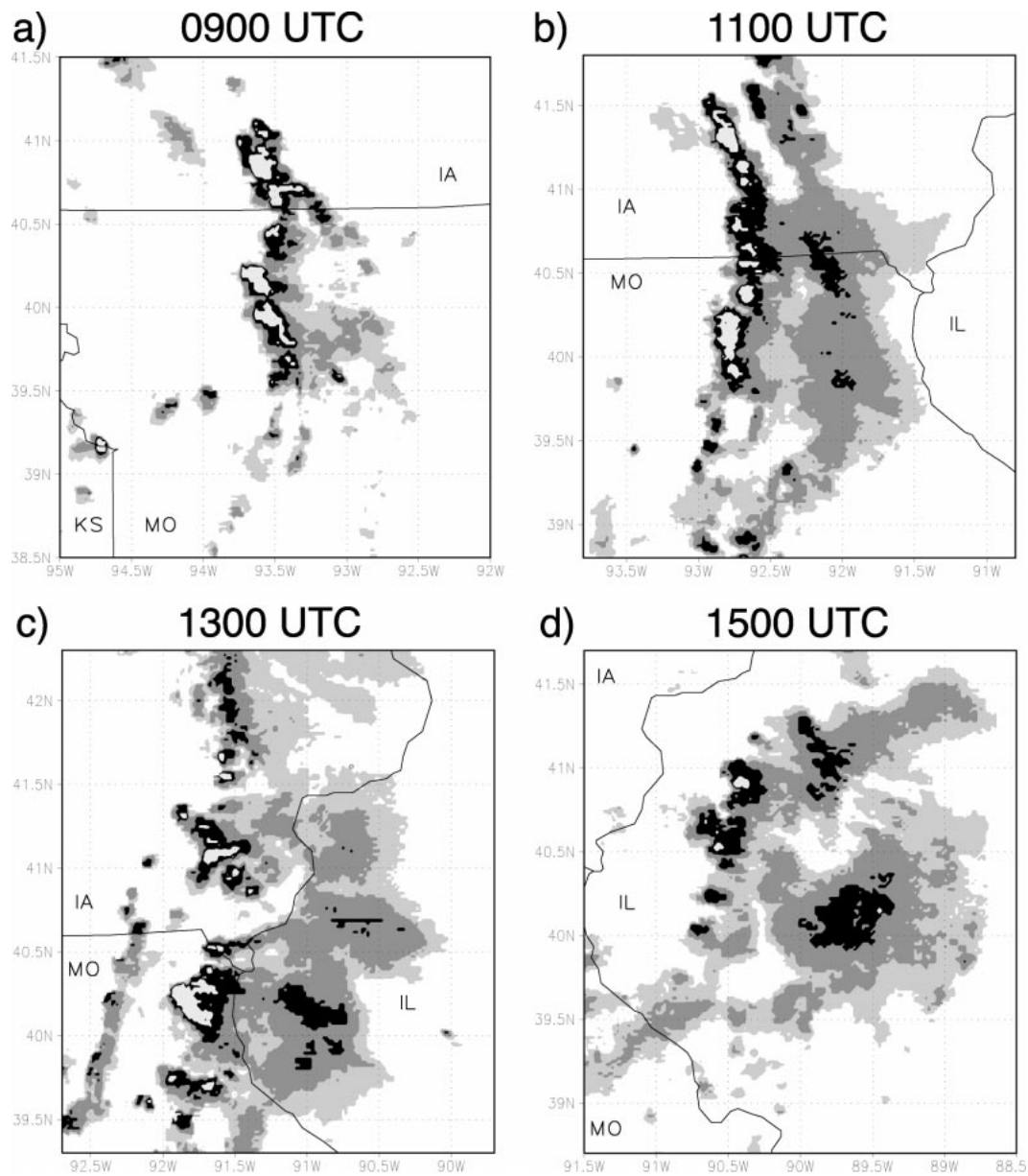
FIG. 13. For 18 May 1997 LS MCS, radar depiction of life cycle at selected times. Reflectivities shaded as in Fig. 5.

upglide over the surface cold dome, when superposed with the pocket of enhanced lower-tropospheric θ_e and any solenoidal circulation caused by the baroclinic zone, was able to lift parcels to their levels of free convection and initiate the line of cells. A similar mechanism was proposed by Maddox et al. (1979) for flash floods and by Fritsch et al. (1994) for mesoscale convective vortex regeneration. The MCS's initial and subsequent orientation was nearly north–south, perpendicular to the temperature gradient (near the Kansas–Missouri border) set up by the previous thunderstorm outflow. By 0800 UTC, the line of convective cells met the 100-km length criterion for MCSs in this study. Even at this earliest stage,

the stratiform rainfall extended eastward of the convective line.

What was initially a line of five convective cores with a small plume of preline rain lengthened and filled in between 0800 and 1000 UTC (Fig. 13a). The convective cells elongated toward the east, perhaps indicating an eastward (storm relative) movement of decaying precipitation cores. Meanwhile, the leading stratiform rain region continued to extend farther to the east of the convective line, preceding its entire north–south extent. By 1100 UTC, along the entire extent of the line, the region of stratiform rain was separated from the deep convective cells by a transition zone (Fig. 13b). Small
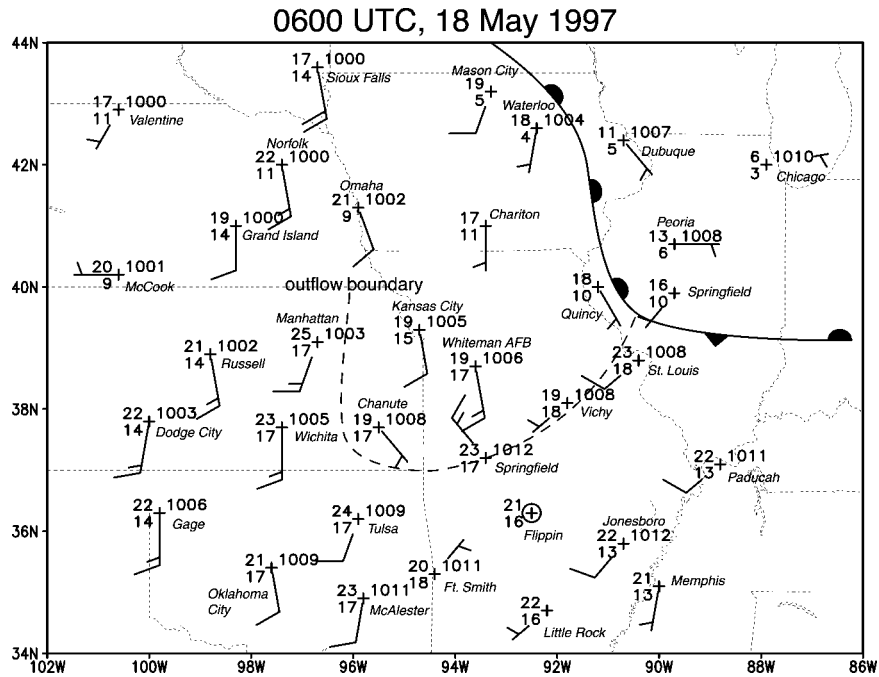
FIG. 14. Surface analysis for 0600 UTC 18 May 1997: temperatures and dewpoint temperatures in °C, MSL pressures in hPa, and wind barbs: barb = 5 m s⁻¹, half barb = 2.5 m s⁻¹.
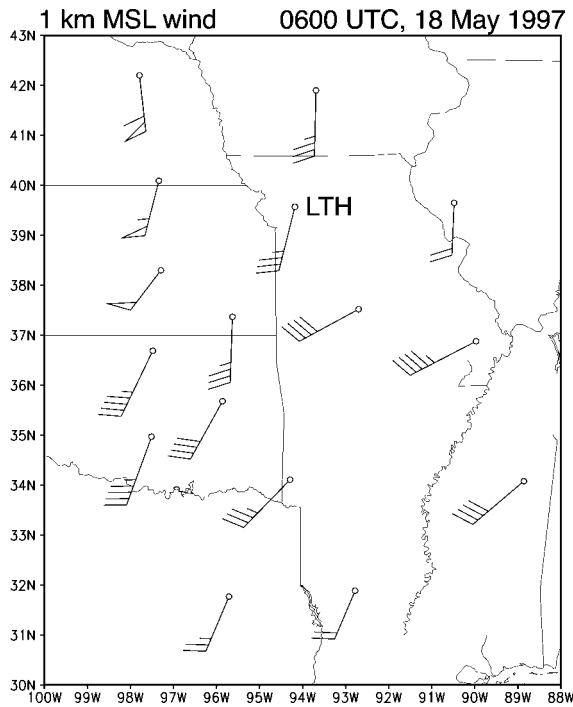

FIG. 15. The 1000 m MSL constant-height NOAA Profiler Network wind barbs at 0600 UTC 18 May 1997: flag = 25 m s⁻¹, barb = 5 m s⁻¹, half barb = 2.5 m s⁻¹. Position of Lathrop, MO (LTH), wind profiler is indicated.

and Houze (1985) discussed such an arrangement of precipitation for a TS system. It is unclear whether their model can be reversed in order to explain the transition zone observed in the 18 May 1997 LS MCS. At 1100 UTC the MCS's convective line reached its maximum horizontal extent and attained its most archetypal reflectivity signature. For this time, therefore, we analyzed the meso-β and meso-α-scale features associated with the maintenance of the LS MCS.

Interestingly, winds immediately ahead of and behind the 18 May 1997 MCS were southerly, with fairly uniform temperatures and dewpoints between the outflow boundary to its south and the stationary front to its north and east (Fig. 17). It is therefore unclear from whence surface air arrived at the updraft towers and to what degree it represented positive buoyancy. Given the MCS's eastward movement, surface storm-relative flow toward the convective line apparently passed through the preline rain region. Additionally, relatively little or no surface wind convergence was evident near the location of the convective line (Fig. 17), although data are admittedly sparse. This case may be analogous to the MCCs studied by Maddox (1983), which were frequently decoupled from the surface layer; however, we lack sufficient surface and upper air data to test this hypothesis. At 1200 UTC (a time at which NCEP reanalysis data were available), the largest lower-tropospheric (925–850 hPa) θ_e near the MCS was to its rear (Fig. 18). The storm-relative winds at LTH displayed a westerly component, suggesting the possibility that lower-tropospheric high-θ_e air was flowing into the trailing
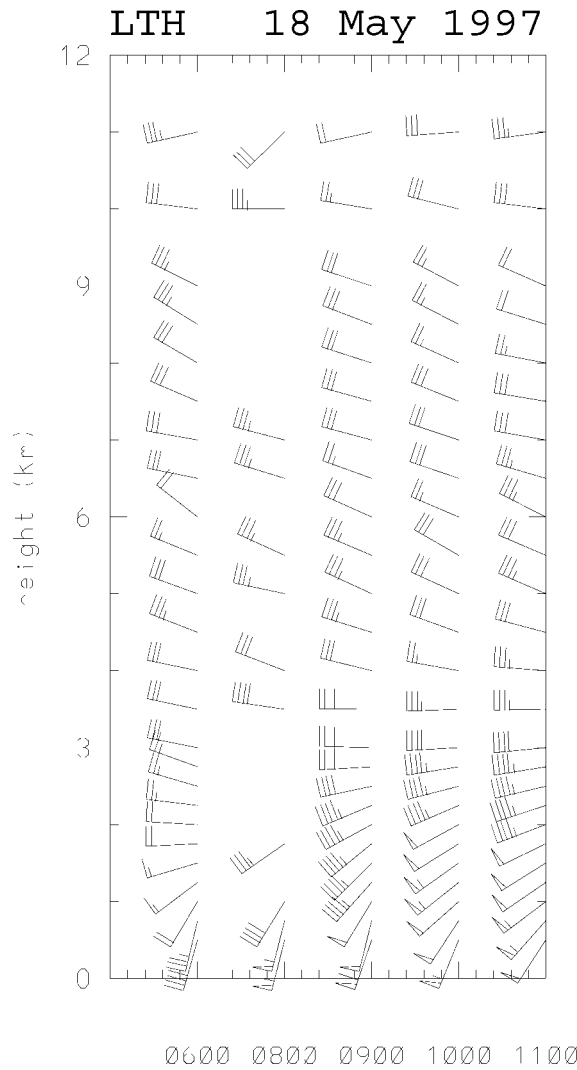
LTH 18 May 1997

FIG. 16. Time series of hourly wind profiles from LTH on 18 May 1997. All times are UTC. Altitudes are above ground level: station elevation is 297 m MSL. Missing barbs indicate data failing quality control checks. At 0700 UTC, all data failed quality control: flag = 25 m s⁻¹, barb = 5 m s⁻¹, half barb = 2.5 m s⁻¹. The profiler's location is shown in Figs. 15 and 18.

edge of the convective line. Such elevated rear inflow would both avoid contamination from the leading stratiform rain region and eliminate the need for less-buoyant surface air that had been previously processed by an earlier MCS.

The convective system weakened after 1200 UTC, and after 1400 UTC it no longer met the length criterion for MCSs in this study (cf. Figs. 13c,d). A dry trough (Hobbs et al. 1996) moved eastward across Kansas on 18 May, nearing Kansas City, Missouri, around 1200 UTC and leaving decreased lower-tropospheric θ_e in its wake. Had the dry air moved sufficiently far eastward to interact with the MCS (a speculation not confirmable by the coarse raob network), the buoyancy of updrafts would have been decreased while evaporation of the
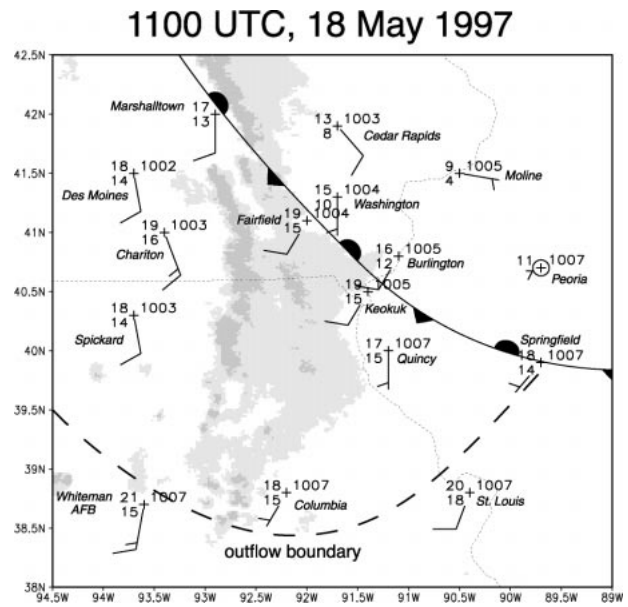

FIG. 17. Surface analysis for 1100 UTC 18 May 1997: temperatures and dewpoint temperatures in °C, MSL pressures in hPa, and wind barbs. Radar reflectivity is shaded. Wind barb = 5 m s⁻¹, half barb = 2.5 m s⁻¹. Light shading, reflectivities 20–40 dBZ; dark shading, reflectivities ≥40 dBZ.
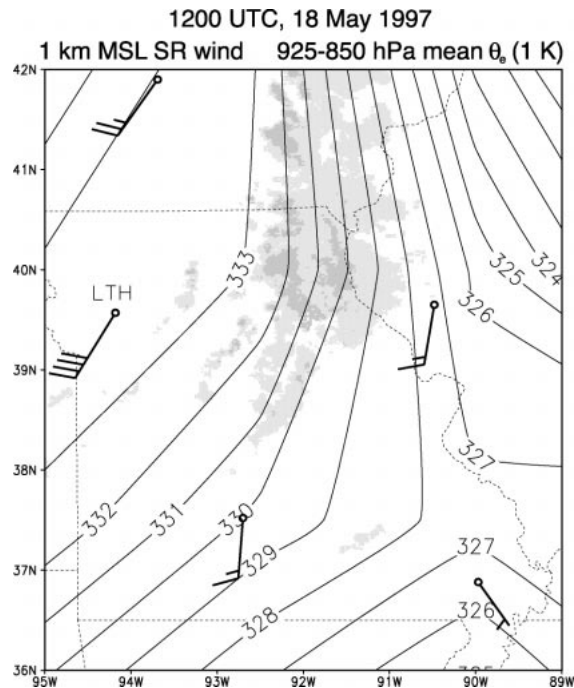

FIG. 18. The 1000 m MSL constant-height NOAA Profiler Network storm-relative wind barbs using storm motion of 14 m s⁻¹ from 260°, NCEP reanalysis 925–850-hPa layer mean equivalent potential temperature (K, contours), and radar reflectivity for 1200 UTC 18 May 1997: barb = 5 m s⁻¹, half barb = 2.5 m s⁻¹. Light shading, reflectivities 20–40 dBZ; dark shading, reflectivities ≥40 dBZ. Position of LTH wind profiler is indicated.

cloud would have increased. In addition, turbulent mixing with less buoyant air at lower levels (due to an early morning increase in surface heat flux) may have further diminished updraft parcels' buoyancy.

In the present case study, the upper-tropospheric winds (as observed at LTH, Fig. 16) were nearly identical to the MCS motion vector, yielding little storm-relative flow above roughly 4 km above ground level. It is therefore unclear what role was played by upper-tropospheric advection of hydrometeors in the leading stratiform distribution of the 18 May 1997 MCS. This finding is inconsistent with the mean storm-relative winds for LS cases found in section 7 (Fig. 12). As well, the upper-tropospheric vertical shear at LTH was fairly weak; the winds were nearly constant in speed and direction above 5 km. Therefore, the explanation given by Grady and Verlinde (1997) for a squall line with LS rain may not apply to the 18 May 1997 MCS. Notably, the lower-tropospheric westerly storm-relative flow was markedly stronger for this case than the LS mean. Perhaps downgradient vertical mixing of rear-to-front lower-tropospheric momentum accounted for some additional component of forward hydrometeor advection by the midlevel flow. However, LeMone (1983) showed that lines of cumulonimbi with trailing stratiform rain may transport momentum upgradient. The correct sign for momentum transport in LS MCSs is uncertain at this time. We hypothesize that the forward movement of precipitation from the convective line may have been enhanced by the establishment of a deep slantwise solenoidal circulation associated with the outflow boundary near the Kansas–Missouri border. This is a concept familiar for TS MCSs: Houze et al. (1989) related the ascending front-to-rear flow in a mature TS line to such a circulation. As the positions of cold outflow and warm lower-tropospheric air for the 18 May 1997 MCS were roughly reversed from the Houze et al. (1989) example, we believe it is possible that such a solenoid was important in determining the precipitation archetype in a sense opposite that of the typical TS MCS. More detailed observations are needed to evaluate the validity of the above processes as reasons for LS rainfall.

b. 26 May 1996: Parallel stratiform

Early on 26 May 1996, a PS MCS formed along the Texas–New Mexico border and slowly traversed the southern Texas Panhandle (cf. Fig. 19). During its lifetime of approximately 9 h, the MCS was oriented from southwest to northeast, with its stratiform rain moving parallel to the line toward the northeast.

Associated with previous thunderstorms over the Texas Panhandle was a broad surface cold pool, demarked by an outflow boundary that extended roughly from Hobbs, New Mexico, through Childress, Texas, and Gage, Oklahoma, to Dodge City, Kansas (Fig. 20). At 0300 UTC, a new elongated reflectivity core developed near Hobbs (not shown), approximately at the intersec-

tion of the aforementioned outflow boundary and a synoptic dryline, and almost immediately it met the MCS length criterion for this study. The initial orientation of the reflectivity core was from southwest to northeast, or roughly parallel to the preexisting outflow boundary.

The 0000 UTC Midland, Texas, sounding reveals a great deal about the general environment within which the MCS developed and evolved (Fig. 21). While the lower-tropospheric winds veered approximately 60° below 750 hPa, there was relatively little middle- and upper-tropospheric directional shear. Since the convective line was oriented roughly southwest to northeast this wind profile represented strong lower-tropospheric inflow along the eastern edge of the line, with very deep and fairly strong (25 m s^{-1} near 500 hPa, >40 m s^{-1} above 300 hPa) middle- and upper-tropospheric flow parallel to the line. From the standpoint of pure advection of hydrometeors (previously discussed in section 7), this scenario appears to be ideal for the PS class. As well, the relatively dry air aloft at Midland suggests the possibility for deep downdrafts due to evaporative and sublimative cooling. Therefore, a potential mechanism was in place for maintenance of the cold surface outflow air, which apparently played some role in the continuing orientation of the MCS.

As the reflectivity cores amalgamated between 0500 and 0700 UTC (Fig. 19a), the stratiform rain associated with each echo entity, and with the entire region of convection, was moving northeastward, parallel to the elongated linear elements. By 0800 UTC the mergers had rendered a predominant convective line centered at 33.7°N, 102°W and a thin band of stratiform rain extending northeastward (Fig. 19b). By 1000 UTC, the convective line had reached its greatest extent and the MCS had its most archetypal appearance (Fig. 19c). Accordingly, we investigated the MCS's near-storm environment at that time.

South-southeasterly storm-relative inflow was occurring ahead of the MCS in the warm sector air (Fig. 22). As might be expected, the highest-θ_e air was located ahead (east) of the convective line (not shown). After 1000 UTC, the MCS began to lose strength, with a declining area of coverage by high reflectivity cores (Fig. 19d). The lysis of the 26 May 1996 PS MCS was apparently related to a decrease in instability of the convective airmass (not shown). The orientation of the MCS throughout its lifetime—parallel to the winds between approximately 700 hPa and the tropopause—as well as its lack of line-normal motion favored advection of hydrometeors in a direction parallel to the line itself.

Had the 26 May 1996 PS MCS moved with a line-normal component, the storm-relative winds would then have had a rearward component, perhaps rendering a different linear MCS mode. Its persistent location is therefore of interest. Topography may have played a role in the general position of the convective line. Running roughly north-northeast to south-southwest through the center of the Texas Panhandle, the Caprock
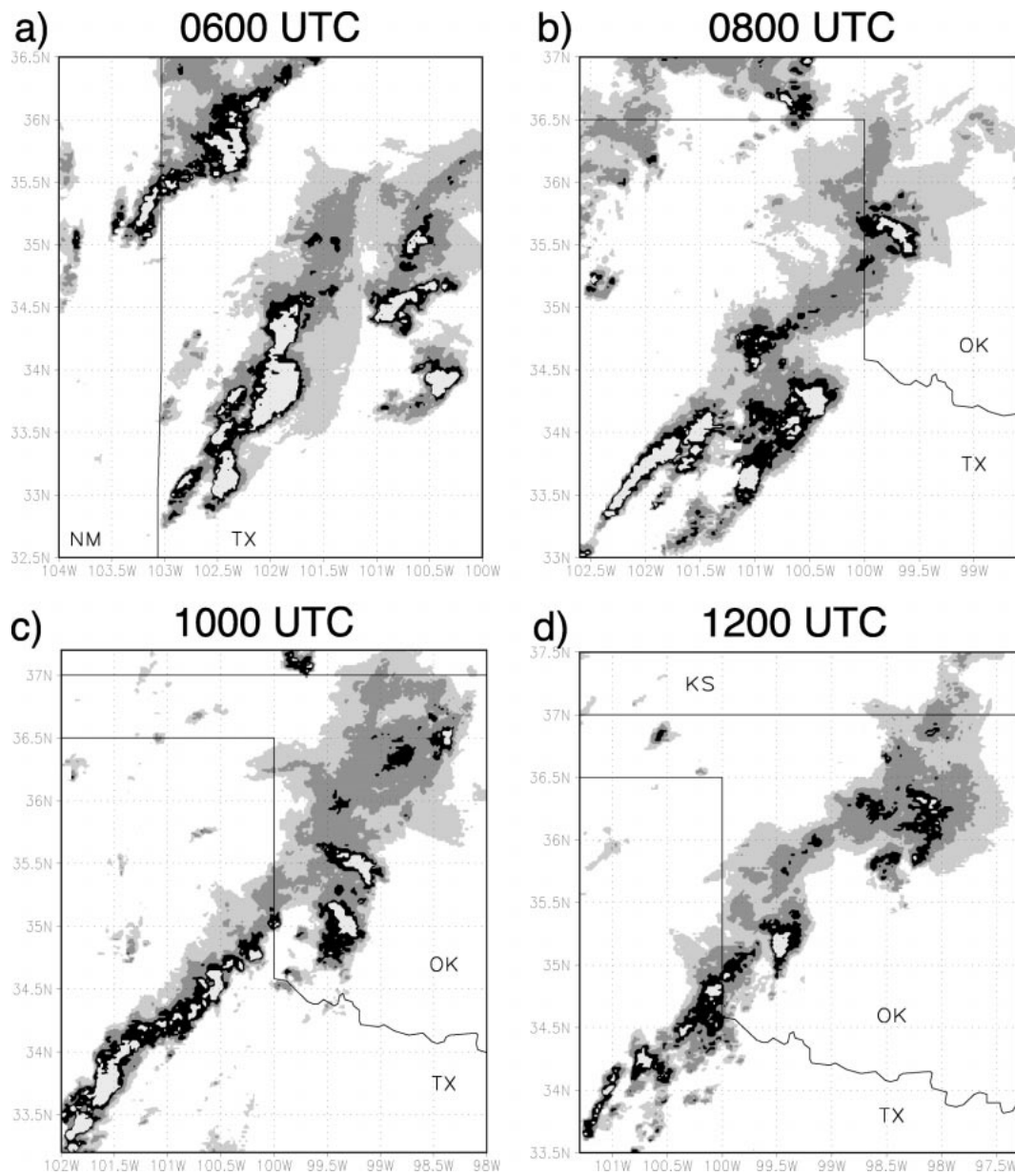
FIG. 19. For 26 May 1996 PS MCS, radar depiction of life cycle at selected times. Reflectivities shaded as in Fig. 5.

Escarpment represents a discontinuity in elevation and terrain. On the high plain above the escarpment, the elevation of Amarillo, Texas, is approximately 1100 m. Due east-southeast of Amarillo, below the escarpment, the elevation of Wheeler, Texas, is approximately 680 m. Although the position of the convective line did not exactly parallel the Caprock Escarpment, orographic lifting of the south-southeasterly flow probably contributed to the location and sustenance of the MCS.

Perhaps more importantly, the preexisting Texas Panhandle outflow boundary—a preferred location for convergence along which the convective cells were aligned—moved very little during the 26 May 1996 MCS's lifetime. While the outflow represented a significant surface temperature gradient, its surface potential temperature (θ) gradient was relatively weaker owing to the irregular terrain. The speed at which a surface cold pool expands can be likened to that of a density current (Charba 1974), which is a function of the magnitude of the negative density (or, neglecting moisture, θ) perturbation of the outflowing fluid. While θ of the observed 1000 UTC surface outflow was 6°C less than that of the air to its south (i.e., at Midland), it was only 1°–3°C less than that of the air to its east (i.e., at Oklahoma City, Wichita Falls, Abilene), implying a less vigorous advancement. Further, Simpson and Britter
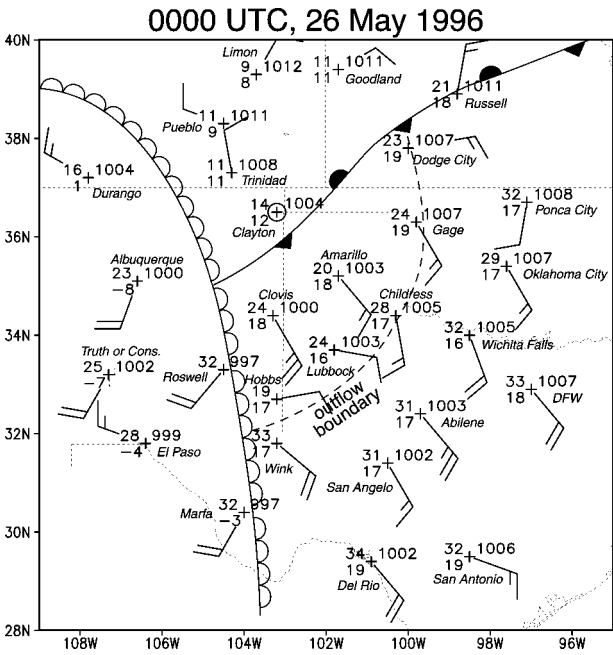
FIG. 20. Same as Fig. 14 but for 0000 UTC 26 May 1996.

(1980) have shown that opposing environmental flow can considerably retard the progress of density currents. In such a manner, the persistent south-southeasterly winds over central Texas may have additionally contributed to the relative lack of motion of the outflow. Finally, the deep-tropospheric line-parallel environmental winds would provide negligible line-normal steering flow. As a result, the 26 May 1996 MCS apparently had little impetus to move away from the persistent convergence along the quasi-stationary outflow boundary. Indeed, between 0700 and 0800 UTC, cells that moved east of the main line appeared to dissipate while the intense reflectivity cores remained near the outflow boundary and escarpment. The dynamical scenario described above would dictate a fairly consistent orientation for the convective line throughout. Because the MCS's orientation was parallel to the strong upper-level winds, hydrometeors were advected along the line rather than perpendicular to it.

The 26 May 1996 MCS was relatively stationary; however, should a PS MCS move more rapidly, the same arguments can be applied to the storm-relative flow (therefore, PS MCSs can and do occur apart from the 26 May 1996 scenario). Skamarock et al. (1994) argued
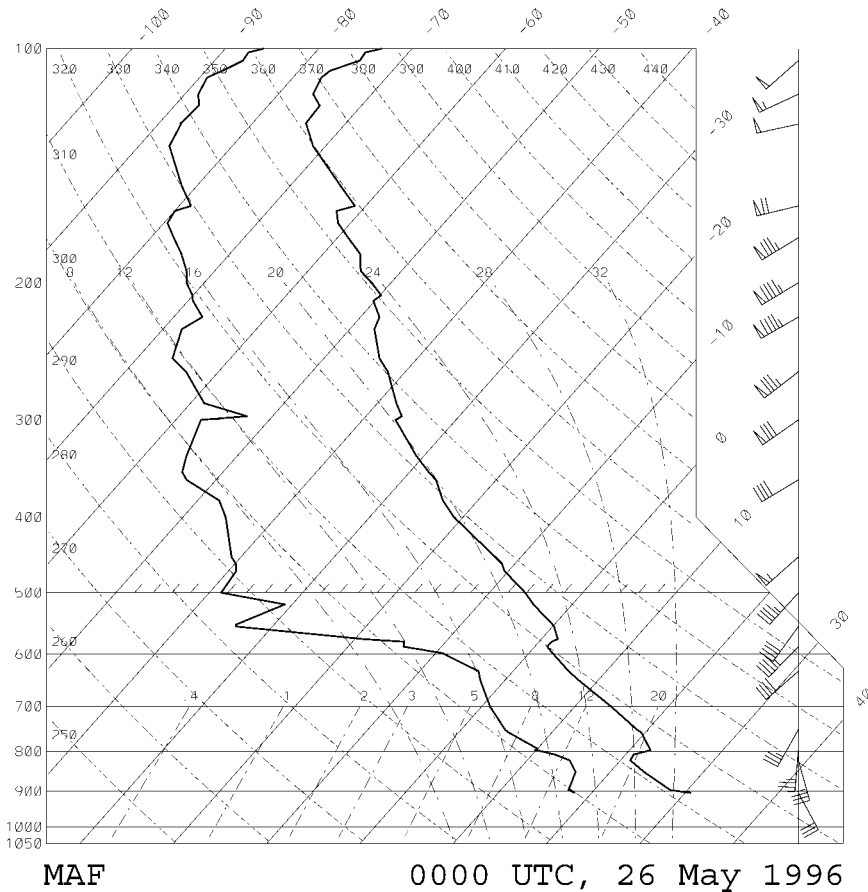

FIG. 21. Skew T–log$p$ plot of rawinsonde observation from Midland, TX (MAF), at 0000 UTC 26 May 1996.
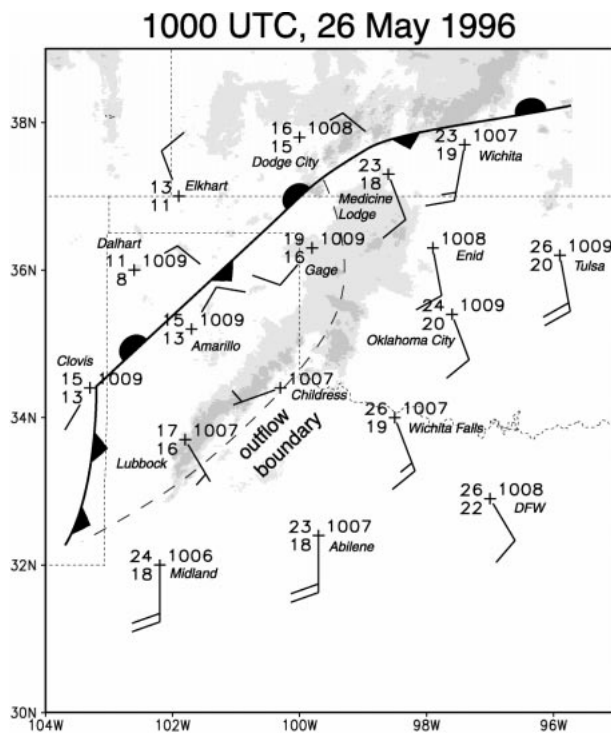
FIG. 22. Same as Fig. 17 but for 1000 UTC 26 May 1996.

that hydrometeors aloft usually have some northward displacement (to the left of the storm's motion vector) due to Coriolis effects, which could also play a role in the PS precipitation distribution. From the 26 May 1996 MCS we infer that the orientation of low-level boundaries may be important to the prolonged orientation of PS convective lines in a fashion parallel to the middle- and upper-tropospheric winds. For the 26 May 1996 MCS, a fortuitous collocation of previous thunderstorm outflows and the Caprock Escarpment provided a linear trigger roughly parallel to the upper-level flow.

LeMone et al. (1998) found that tropical convective lines were often aligned with the 800–400-hPa vector wind difference when it was ''strong'' ($\geq$5 m s^{-1}). Such correlations do not appear to hold as well in the mid-latitudes, no doubt due in part to the variety of lower-tropospheric convergence boundaries along which mid-latitude linear MCSs are initiated and tend to align. This discrepancy is evinced by the 26 May 1996 PS MCS, whose midlevel shear vector pointed eastward but whose orientation was NE–SW along an outflow boundary. Indeed, LeMone et al. (1998) found that TOGA COARE MCSs forced along preexistent cold pools in general had no preferred orientation with respect to the environmental shear (cf. their Table 3). If the orientation of the triggering boundary is a constraint upon whether a case becomes PS, then it is not surprising that they are less frequent than TS cases. The appropriate alignment of a boundary with the upper-level winds may be

somewhat unusual (PS cases accounted for 19% of all MCSs in this study).

9. Synthesis of results

We have defined midlatitude *linear mesoscale convective systems* as convective lines, with their attendant stratiform precipitation, that exist for longer than 3 h (a timescale of f^{-1}) and extend more than 100 km horizontally (a length scale of Uf^{-1}). Using national 2-km base scan reflectivity data, we identified 88 linear mesoscale convective systems over the central plains during May 1996 and May 1997. The mean synoptic environment attending the MCSs in this investigation corresponded well with those discovered in previous studies. In general, convective systems were located in a region of lower-tropospheric warm air advection in advance of an approaching upper-tropospheric short-wave trough, similar to the MCC environments reported by Maddox (1983). It was found that 27% of the studied cases occurred on the cold side of synoptic fronts. The remaining linear *warm sector* MCSs occurred almost exclusively near linear surface boundaries, most frequently near warm or stationary fronts. We therefore conclude that linear triggers are of first-order importance to linearly organized MCSs. Related to this result, linear MCS frequency was maximized when surface cyclones traversed the study region, probably owing to the synoptic-scale boundaries that frequently accompany them. Low-level jets also frequently attended periods of increased activity. A nocturnal maximum in linear MCSs, similar to those discussed by Maddox (1980) and HSD90, was noted during the study period. Additionally, a less well-documented secondary maximum occurred near local sunrise, a phenomenon similar to that observed by Geerts (1998) for the southeastern United States. This result may be relatively new, arising from the use of regional radar data rather than single-site radar data or infrared satellite imagery.

Observation of the radar data revealed three prominent modes of linear MCS precipitation distribution: those with trailing stratiform, leading stratiform, and parallel stratiform. We therefore propose a taxonomy incorporating these three archetypes. Among the 88 cases during May 1996 and May 1997, 51 fit the TS archetype and 17 each fit the LS and PS archetypes (3 were unclassifiable). The prominence of the TS mode confirmed previous findings by HSD90 for Oklahoma. Warm sector TS MCSs persisted the longest of the three classes by nearly a factor of 2 (12.2 h, vs 6.5 and 6.3 h for LS and PS cases, respectively). The TS MCSs also moved the fastest of the linear MCS groups, while LS cases on average moved the slowest. We observed that linear MCSs evolved toward a TS structure at some point in well over half the studied cases.

For warm sector MCSs we utilized rawinsonde, wind profiler, and NCEP reanalysis data to characterize the mean environment near each linear MCS mode. Statis-

tically significant variations in many environmental parameters between the linear MCS classes were noted, supporting the hypothesis that dynamical differences exist between the three archetypes. On average, TS MCSs occurred in more unstable air masses than did LS or PS cases. Based upon prestorm raobs, we found that TS MCSs generally occurred in environments conducive to stronger cold pools than those of PS cases, which in turn occurred in environments conducive to stronger cold pools than those of LS MCSs; thus, the longevities and relative speeds of the three classes may to some degree result from cold pool dynamics. Rearward storm-relative advection of hydrometeors was indicated in the middle troposphere for TS cases, while the reverse was implied for LS MCSs. In some LS MCSs, such as the 18 May 1997 case study presented above, other factors such as downgradient mixing of low-level rear-to-front storm-relative momentum or slantwise solenoidal overturning could also possibly play a role in the forward movement of precipitation. Although the persistence of LS MCSs is somewhat mysterious given that, on average, their inflow passes through a large region of precipitation, one possibility represented by the 18 May 1997 case is that LS MCSs can be sustained by inflow into the rear of their convective lines. Middle-tropospheric storm-relative winds blew along the convective line, on average, for PS cases. In many PS MCSs, as in the 26 May 1996 case studied above, the orientation of the low-level forcing with respect to the environmental flow is probably significant. Due to the variety of lower-tropospheric boundaries along which midlatitude storms are initiated and align, the conclusions of LeMone et al. (1998) regarding tropical MCSs' alignment with the midlevel shear vector may have less applicability in the midlatitudes. We did not find conclusive evidence that the vertical wind shear was significantly different among the three MCS classes, although it may be of importance for some cases (as discussed by Grady and Verlinde 1997). Nor did we discover that LS cases occurred in environments especially conducive to supercells (a possibility entertained by Fankhauser et al. 1992). Our results suggest that the arrangement of stratiform precipitation in linear MCSs is largely related to the storm-relative flow in and near the level of maximum hydrometeor transport [approximately 5–8 km according to Rutledge and Houze (1987)].

10. Future work

The frequency of LS and PS MCSs in this study highlights the need for further investigation of their dynamics and predictability. Information about the prominence of the identified convective modes in other regions of the United States and the world is desirable in order to further qualify the representativeness of this and numerous other Great Plains MCS studies. As well, we omitted non-warm-sector MCSs from our detailed analysis, a void that could be remedied by future work. In addition to further testing of the taxonomy, greater insight into the vertical structure and internal flow features of the LS and PS archetypes is needed. Of particular interest is the manner in which LS MCSs are able to survive inflow of evaporatively cooled air toward their convective towers. Future case studies should include multiple radar elevation scans, as well as range–height indicator imagery, to depict the depth and movement of convective and stratiform hydrometeors. Further, the addition of dual-Doppler radar data, when available, will help to demonstrate recurrent flow features for LS and PS MCSs, much as has been done for many TS cases (e.g., Biggerstaff and Houze 1991). Only with full knowledge of these three-dimensional structures can robust conceptual models for the less-studied archetypes be developed. A rigorous conceptual model for each of the three linear MCS archetypes (only the TS is currently well known) will improve recognition and forecasting of linear MCS modes, as well as numerical model parameterizations of mesoscale organized convection and its attendant effects. Finally, our overview of national radar data suggests that, during May 1996 and May 1997, linear and nonlinear MCSs occurred with approximately equal frequency. Because of the differing transports associated with linear and nonlinear convection (LeMone and Moncrieff 1994), a more detailed study of the midlatitude ratio of linear to nonlinear MCSs would make clearer the role of the systems discussed in this paper, and would be of great interest to forecasters and numerical modelers alike.

11. Summary

This study cataloged and analyzed 88 linear MCSs from the central plains in May 1996 and May 1997. Our main findings include the following.

- There exist three distinct modes of linear MCS: trailing stratiform (TS, $\approx$60% of the cases), leading stratiform (LS, $\approx$20% of the cases), and parallel stratiform (PS, $\approx$20% of the cases).
- The TS MCSs experienced front-to-rear storm-relative winds throughout their depth, moved rapidly, and were the longest lived of the three classes.
- The LS MCSs experienced weak middle- and upper-tropospheric rear-to-front storm-relative winds, moved slowly, and persisted for approximately half as long as TS MCSs.
- The PS MCSs experienced significant middle- and upper-tropospheric line-parallel storm-relative winds, moved more rapidly than LS MCSs but less rapidly than TS MCSs, and persisted for approximately half as long as TS MCSs.
- At some point in their life cycle, a majority of MCSs evolve toward TS structure.
- The synoptic conditions associated with linear MCSs in this study largely resembled those discovered by

previous authors (e.g., Maddox 1983; Bluestein and Jain 1985; Kane et al. 1987).
• In addition to a nocturnal maximum in linear MCS frequency, a secondary near-sunrise mode existed similar to that documented by Geerts (1998).

One case study suggests that for PS MCSs, the orientation of a linear trigger to the tropospheric wind profile may be of first-order importance, while another suggests that LS MCSs may be sustained in a variety of ways, including inflow from the rear.

REFERENCES

Alexander, G. D., and G. S. Young, 1992: The relationship between EMEX mesoscale precipitation feature properties and their environmental characteristics. *Mon. Wea. Rev.,* **120,** 554–564.

Barnes, G. M., and K. Sieckman, 1984: The environment of fast- and slow-moving tropical mesoscale convective cloud lines. *Mon. Wea. Rev.,* **112,** 1782–1794.

Barth, M. F., R. B. Chadwick, and D. W. van de Kamp, 1994: Data processing algorithms used by NOAA's wind profiler demonstration network. *Ann. Geophys.,* **12,** 518–528.

Belair, S., D.-L. Zhang, and J. Mailhot, 1995: Numerical prediction of an intense convective system associated with the July 1987 Montreal flood. Part II: A trailing stratiform rainband. *Atmos.– Ocean,* **33,** 475–500.

Biggerstaff, M. I., and R. A. Houze Jr., 1991: Kinematic and precipitation structure of the 10–11 June 1985 squall line. *Mon. Wea. Rev.,* **119,** 3034–3065.

Bjerknes, J., and H. Solberg, 1922: Life cycle of cyclones and the polar front theory of atmospheric circulation. *Geofys. Publ.,* **3** (1), 1–18.

Blanchard, D. O., W. R. Cotton, and J. M. Brown, 1998: Mesoscale circulation growth under conditions of weak inertial instability. *Mon. Wea. Rev.,* **126,** 118–140.

Bluestein, H. B., and C. R. Parks, 1983: Synoptic and photographic climatology of low-precipitation severe thunderstorms in the southern plains. *Mon. Wea. Rev.,* **111,** 2034–2046.

——, and M. H. Jain, 1985: Formation of mesoscale lines of precipitation: Severe squall lines in Oklahoma during the spring. *J. Atmos. Sci.,* **42,** 1711–1732.

——, G. T. Marx, and M. H. Jain, 1987: Formation of mesoscale lines of precipitation: Nonsevere squall lines in Oklahoma during the spring. *Mon. Wea. Rev.,* **115,** 2719–2727.

Braun, S. A., and R. A. Houze Jr., 1995: Melting and freezing in a mesoscale convective system. *Quart. J. Roy. Meteor. Soc.,* **121,** 55–77.

——, and ——, 1997: The evolution of the 10–11 June 1985 PRE-

STORM squall line: Initiation, development of rear inflow, and dissipation. *Mon. Wea. Rev.,* **125,** 478–504.

Caniaux, G., J. P. Lafore, and J.-L. Redelsperger, 1995: A numerical study of the stratiform region of a fast-moving squall line. Part II: Relationship between mass, pressure, and momentum fields. *J. Atmos. Sci.,* **52,** 331–352.

Charba, J., 1974: Application of gravity current model to analysis of squall-line gust front. *Mon. Wea. Rev.,* **102,** 140–156.

Colman, B. R., 1990: Thunderstorms above frontal surfaces in environments without positive CAPE. Part I: A climatology. *Mon. Wea. Rev.,* **118,** 1103–1121.

Crook, N. A., and M. W. Moncrieff, 1988: The effect of large-scale convergence on the generation and maintenance of deep moist convection. *J. Atmos. Sci.,* **45,** 3606–3624.

Doswell, C. A., III, H. E. Brooks, and R. A. Maddox, 1996: Flash flood forecasting: An ingredients-based methodology. *Wea. Forecasting,* **11,** 560–581.

Emanuel, K. A., 1986: Overview and definition of mesoscale meteorology. *Mesoscale Meteorology and Forecasting,* P. S. Ray, Ed., Amer. Meteor. Soc., 1–17.

Fankhauser, J. C., G. M. Barnes, and M. A. LeMone, 1992: Structure of a midlatitude squall line formed in strong unidirectional shear. *Mon. Wea. Rev.,* **120,** 237–260.

Fovell, R. G., and P. S. Dailey, 1995: The temporal behavior of numerically simulated multicell-type storms. Part I: Modes of behavior. *J. Atmos. Sci.,* **52,** 2073–2095.

Fritsch, J. M., J. D. Murphy, and J. S. Kain, 1994: Warm core vortex amplication over land. *J. Atmos. Sci.,* **51,** 1780–1807.

Gallus, W. A., and R. H. Johnson, 1995a: The dynamics of circulations within the trailing stratiform regions of squall lines. Part I: The 10–11 June PRE-STORM system. *J. Atmos. Sci.,* **52,** 2161–2187.

——, and ——, 1995b: The dynamics of circulations within the trailing stratiform regions of squall lines. Part II: Influence of the convective line and ambient environment. *J. Atmos. Sci.,* **52,** 2188–2211.

Geerts, B., 1998: Mesoscale convective systems in the southeast United States during 1994–95: A survey. *Wea. Forecasting,* **13,** 860–869.

Grady, R. L., and J. Verlinde, 1997: Triple-Doppler analysis of a discretely propagating, long-lived, high plains squall line. *J. Atmos. Sci.,* **54,** 2729–2748.

Gray, W. M., and R. W. Jacobson Jr., 1977: Diurnal variation of deep cumulus convection. *Mon. Wea. Rev.,* **105,** 1171–1188.

Hane, C. E., and D. P. Jorgensen, 1995: Dynamic aspects of a distinctly three-dimensional mesoscale convective system. *Mon. Wea. Rev.,* **123,** 3194–3214.

Hilgendorf, E. R., and R. H. Johnson, 1998: A study of the evolution of mesoscale convective systems using WSR-88D data. *Wea. Forecasting,* **13,** 437–452.

Hobbs, P. V., J. D. Locatelli, and J. E. Martin, 1996: A new conceptual model for cyclones generated in the lee of the Rocky Mountains. *Bull. Amer. Meteor. Soc.,* **77,** 1169–1178.

Houze, R. A., Jr., 1993: *Cloud Dynamics.* Academic Press, 573 pp.

——, S. A. Rutledge, M. I. Biggerstaff, and B. F. Smull, 1989: Interpretation of Doppler weather radar displays of midlatitude mesoscale convective systems. *Bull. Amer. Meteor. Soc.,* **70,** 608–619.

——, B. F. Smull, and P. Dodge, 1990: Mesoscale organization of springtime rainstorms in Oklahoma. *Mon. Wea. Rev.,* **118,** 613–654.

Huschke, R. E., Ed., 1959: *Glossary of Meteorology.* Amer. Meteor. Soc., 638 pp.

Kalnay, E., and Coauthors, 1996: The NCEP/NCAR 40-Year Reanalysis Project. *Bull. Amer. Meteor. Soc.,* **77,** 437–471.

Kane, R. J., Jr., C. R. Chelius, and J. M. Fritsch, 1987: Precipitation characteristics of mesoscale convective weather systems. *J. Climate Appl. Meteor.,* **26,** 1345–1357.

Knupp, K. R., B. Geerts, and S. J. Goodman, 1998a: Analysis of a small, vigorous mesoscale convective system in a low-shear en-

vironment. Part I: Formation, radar echo structure, and lightning behavior. *Mon. Wea. Rev.,* **126,** 1812–1836.

——, ——, and J. D. Tuttle, 1998b: Analysis of a small, vigorous mesoscale convective system in a low-shear environment. Part II: Evolution of the stratiform precipitation and mesoscale flows. *Mon. Wea. Rev.,* **126,** 1837–1858.

LeMone, M. A., 1983: Momentum transport by a line of cumulonimbus. *J. Atmos. Sci.,* **40,** 1815–1834.

——, and M. W. Moncrieff, 1994: Momentum and mass transport by convective bands: Comparisons of highly idealized dynamical models to observations. *J. Atmos. Sci.,* **51,** 281–305.

——, E. J. Zipser, and S. B. Trier, 1998: The role of environmental shear and thermodynamic conditions in determining the structure and evolution of mesoscale convective systems during TOGA COARE. *J. Atmos. Sci.,* **55,** 3493–3518.

Loehrer, S. M., and R. H. Johnson, 1995: Surface pressure and precipitation life cycle characteristics of PRE-STORM mesoscale convective systems. *Mon. Wea. Rev.,* **123,** 600–621.

Ludlam, F. H., 1963: Severe local storms: A review. *Severe Local Storms. Meteor. Monogr.,* No. 27, Amer. Meteor. Soc., 1–30.

Maddox, R. A., 1980: Mesoscale convective complexes. *Bull. Amer. Meteor. Soc.,* **61,** 1374–1387.

——, 1983: Large-scale meteorological conditions associated with midlatitude mesoscale convective complexes. *Mon. Wea. Rev.,* **111,** 1475–1493.

——, C. F. Chappell, and L. R. Hoxit, 1979: Synoptic and meso-α scale aspects of flash flood events. *Bull. Amer. Meteor. Soc.,* **60,** 115–123.

Mapes, B. E., 1993: Gregarious tropical convection. *J. Atmos. Sci.,* **50,** 2026–2037.

McAnelly, R. L., and W. R. Cotton, 1986: Meso-β-scale characteristics of an episode of meso-α-scale convective complexes. *Mon. Wea. Rev.,* **114,** 1740–1770.

Miller, P. A., M. F. Barth, J. R. Smart, and L. A. Benjamin, 1997: The extent of bird contamination in the hourly winds measured by the NOAA profiler network: Results before and after implementation of the new bird contamination quality control check. Preprints, *First Symp. on Integrated Observing Systems,* Long Beach, CA, Amer. Meteor. Soc., 138–144.

Moncrieff, M. W., 1992: Organized convective systems: Archetypal dynamical models, mass and momentum flux theory, and parameterization. *Quart. J. Roy. Meteor. Soc.,* **118,** 819–850.

Newton, C. W., 1966: Circulations in large sheared cumulonimbus. *Tellus,* **18,** 699–712.

——, and H. R. Newton, 1959: Dynamical interactions between large convective clouds and environment with vertical shear. *J. Meteor.,* **16,** 483–496.

——, and J. C. Fankhauser, 1964: On the movements of convective storms, with emphasis on size discrimination in relation to water-budget requirements. *J. Appl. Meteor.,* **3,** 651–668.

Nicholls, M. E., R. A. Pielke, and W. R. Cotton, 1991: Thermally forced gravity waves in an atmosphere at rest. *J. Atmos. Sci.,* **48,** 1869–1884.

Orlanksi, I., 1975: A rational subdivision of scales for atmospheric processes. *Bull. Amer. Meteor. Soc.,* **56,** 527–530.

Parker, M. D., 1999: May 1996 and May 1997 linear mesoscale convective systems of the Central Plains: Synoptic meteorology and a reflectivity-based taxonomy. Dept. of Atmospheric Science Paper No. 675, Colorado State University, Fort Collins, CO, 185 pp. [Available from Dept. of Atmospheric Science, Colorado State University, Fort Collins, CO 80523.]

Purdom, J. F. W., 1986: Convective-scale interaction: Arc cloud lines and the development and evolution of deep convection. Dept. of Atmospheric Science Paper No. 408, Colorado State University, Fort Collins, CO, 197 pp. [Available from Dept. of At-

mospheric Science, Colorado State University, Fort Collins, CO 80523.]

Rasmussen, E. N., and R. B. Wilhelmson, 1983: Relationships between storm characteristics and 1200 GMT hodographs, low-level shear, and stability. Preprints, *13th Conf. on Severe Local Storms,* Tulsa, OK, Amer. Meteor. Soc., J5–J8.

——, and J. M. Straka, 1998: Variations of supercell morphology. Part I: Observations of the role of upper-level storm-relative flow. *Mon. Wea. Rev.,* **126,** 2406–2421.

Rodgers, D. M., K. W. Howard, and E. C. Johnston, 1983: Mesoscale convective complexes over the United States during 1982. *Mon. Wea. Rev.,* **111,** 2363–2369.

Rotunno, R., J. B. Klemp, and M. L. Weisman, 1988: A theory for strong, long-lived squall lines. *J. Atmos. Sci.,* **45,** 463–485.

Rutledge, S. A., 1986: Diagnostic modeling study of the stratiform region associated with a tropical squall line. *J. Atmos. Sci.,* **43,** 1356–1377.

——, and R. A. Houze Jr., 1987: Diagnostic modeling study of the trailing stratiform region of a midlatitude squall line. *J. Atmos. Sci.,* **44,** 2640–2656.

Sanders, F., 1999: A proposed method of surface map analysis. *Mon. Wea. Rev.,* **127,** 945–955.

——, and C. A. Doswell III, 1995: A case for detailed surface analysis. *Bull. Amer. Meteor. Soc.,* **76,** 505–521.

Schiesser, H. H., R. A. Houze Jr., and H. Huntrieser, 1995: The mesoscale structure of severe precipitation systems in Switzerland. *Mon. Wea. Rev.,* **123,** 2070–2097.

Schmidt, J. M., and W. R. Cotton, 1990: Interactions between upper and lower tropospheric gravity waves on squall line structure and maintenance. *J. Atmos. Sci.,* **47,** 1205–1222.

Simpson, J. E., and R. E. Britter, 1980: Laboratory model of an atmospheric mesofront. *Quart. J. Roy. Meteor. Soc.,* **106,** 485–500.

Skamarock, W. C., M. L. Weisman, and J. B. Klemp, 1994: Three-dimensional evolution of simulated long-lived squall lines. *J. Atmos. Sci.,* **51,** 2563–2584.

Smull, B. F., and R. A. Houze Jr., 1985: A midlatitude squall line with a trailing region of stratiform rain: Radar and satellite observations. *Mon. Wea. Rev.,* **113,** 117–133.

Trier, S. B., and D. B. Parsons, 1993: Evolution of environmental conditions preceding the development of a nocturnal mesoscale convective complex. *Mon. Wea. Rev.,* **121,** 1078–1098.

Tripoli, G. J., 1987: Scale interaction within a developing mesoscale convective system. Preprints, *Third Conf. of Mesoscale Processes,* Vancouver, BC, Canada, Amer. Meteor. Soc., 131–132.

Uccellini, L. W., and D. R. Johnson, 1979: The coupling of upper and lower tropospheric jet streaks and implications for the development of severe convective storms. *Mon. Wea. Rev.,* **107,** 682–703.

Wallace, J. M., 1975: Diurnal variations in precipitation and thunderstorm frequency over the conterminous United States. *Mon. Wea. Rev.,* **103,** 406–419.

Weber, B. L., D. B. Wuertz, D. C. Welsh, and R. McPeek, 1993: Quality control for profiler measurements of winds and RASS temperatures. *J. Atmos. Oceanic Technol.,* **10,** 452–464.

Wilczak, J. M., and Coauthors, 1995: Contamination of wind profiler data by migrating birds: Characteristics of corrupted data and potential solutions. *J. Atmos. Oceanic Technol.,* **12,** 449–467.

Yang, M. J., and R. A. Houze Jr., 1995: Multicell squall-line structure as a manifestation of vertically trapped gravity waves. *Mon. Wea. Rev.,* **123,** 641–661.

——, and ——, 1996: Momentum budget of a squall line with trailing stratiform precipitation: Calculations with a high-resolution numerical model. *J. Atmos. Sci.,* **53,** 3629–3652.

Zipser, E. J., 1982: Use of a conceptual model of the life cycle of mesoscale convective systems to improve very-short-range forecasts. *Nowcasting,* K. Browning, Ed., Academic Press, 191–204.